Conf-9010185--21

ESTIMATION OF FRACTURE TOUGHNESS OF CAST STAINLESS STEELS IN LWR SYSTEMS

CONF-9010185--21

DE91 006636

O. K. Chopra

Materials and Components Technology Division
Argonne National Laboratory
9700 South Cass Avenue
Argonne, Illinois 60439 USA

DISCLAIMER

October 1990

Presented at the Eighteenth Water Reactor Safety Information Meeting, October 22-24, 1990, Rockville, MD.

ESTIMATION OF FRACTURE TOUGHNESS OF CAST STAINLESS STEELS IN LWR SYSTEMS

O. K. Chopra

Materials and Components Technology Division
Argonne National Laboratory
9700 South Cass Avenue
Argonne, Illinois 60439

Abstract

A procedure and correlations are presented for predicting fracture toughness J–R curves and impact strength of aged cast stainless steels from known material information. The "saturation" fracture toughness of a specific cast stainless steel, i.e., the minimum fracture toughness that would ever be achieved for the material after long-term service, is estimated from the degree of embrittlement at saturation. Degree of embrittlement is characterized in terms of room-temperature Charpy-impact energy. The variation of the impact energy at saturation for different materials is described in terms of a material parameter Φ, which is determined from the chemical composition and ferrite morphology. The fracture toughness J–R curve for the material is then obtained from correlations between room-temperature Charpy-impact energy and fracture toughness. Fracture toughness as a function of time and temperature of reactor service is estimated from the kinetics of embrittlement, which is determined from the chemical composition. Examples for estimating impact strength and fracture toughness of cast stainless steel components during reactor service are described. A common "lower-bound" J-R curve for cast stainless steels with unknown chemical composition is also defined.

1. Introduction

Cast duplex stainless steels used in light water reactor (LWR) systems for primary pressure-boundary components such as valve bodies, pump casings, and primary coolant piping, are susceptible to thermal embrittlement at reactor operating temperatures (280–320°C). Aging of cast stainless steels at these temperatures causes an increase in hardness and tensile strength and a decrease in ductility, impact strength, and fracture toughness of the material. Most studies on thermal embrittlement of cast stainless steels involve simulation of end-of-life reactor conditions by accelerated aging at higher temperatures, viz., 400°C, since the time period for operation of power plant (~40 y) is far longer than can generally be considered for laboratory studies. Thus, estimates of the loss of toughness suffered by cast stainless steel components are based on an Arrhenius extrapolation of the high temperature data to reactor operating conditions. A program is being conducted at Argonne National Laboratory (ANL) to investigate the low-temperature embrittlement of cast duplex stainless steels in LWR systems and to evaluate possible remedies for the embrittlement problem in existing and future plants. The scope of the investigation includes the following goals: (1) develop a methodology and correlations for predicting the toughness loss suffered by cast stainless steel components during normal and extended life of LWRs, (2) validate the simulation of in-reactor degradation by accelerated aging, and (3) establish the effects of key compositional and metallurgical variables on the kinetics and extent of embrittlement.

Microstructural and mechanical property data are being obtained on laboratory-aged material from 25 experimental heats (static-cast keel blocks and slabs) and 6 commercial heats (centrifugally cast pipes and a static-cast pump impeller and pump casing ring), as well as on reactor-aged material of CF-3, CF-8, and CF-8M grades of cast stainless steel. The reactor-aged material is from the recirculating-pump cover plate assembly of the KRB reactor, which was in service in Gundremmingen, West Germany for ~12 yr (~8 yr at a service temperature of 280°C). The chemical composition, hardness, and ferrite content and distribution of some of the cast materials are given in Table 1. The data from Charpy-impact, tensile, and J-R curve tests on several heats of cast stainless steel aged up to 30,000 h at temperatures between 290 and 450°C have been presented earlier.[1-4] A preliminary assessment of the processes and significance of the thermal aging in cast stainless steels was also presented.[3,4]

The work at ANL and elsewhere has shown that embrittlement of cast stainless steel components will occur during the reactor life time of 40 years. Different heats exhibit different degrees of embrittlement. In general, the low-carbon CF-3 steels are the most resistant, and the Mo-containing, high-carbon CF-8M steels are the least resistant to embrittlement. The extent of embrittlement increases with an increase in ferrite content.

Embrittlement of cast stainless steels results in a brittle fracture associated with either cleavage of the ferrite or separation of the ferrite/austenite phase boundary. The degree of embrittlement is controlled by the amount of brittle fracture. Cast stainless steels with poor impact strength exhibit >80% brittle fracture. In some cast steels a fraction of the material may fail in a brittle fashion but the surrounding austenite provides ductility and toughness. Such steels have adequate impact strength even after long-term aging. A predominantly brittle failure occurs when either the ferrite phase is continuous, e.g., in cast material with a large ferrite content, or the ferrite/austenite phase boundary provides an easy path for crack propagation, e.g., in high-carbon grades of cast steels with large phase-boundary carbides. Consequently, the amount, size, and distribution of the ferrite phase in the duplex structure and the presence of phase-boundary carbides are important parameters in controlling the degree or extent of embrittlement.

Thermal aging of cast stainless steels at 300 to 450°C leads to precipitation of additional phases in the ferrite matrix, e.g., formation of a Cr-rich α' phase by spinodal decomposition and precipitation of an Ni- and Si-rich G phase, $M_{23}C_6$ carbide, and γ_2 (austenite); and additional precipitation and/or growth of existing carbides at the ferrite/ austenite phase boundaries[5-8]. The additional phases provide the strengthening mechanisms that increase strain hardening and the local tensile stress. Consequently, the critical stress level for brittle fracture is achieved at higher temperatures.

The effects of material variables on the embrittlement of cast stainless steels have been evaluated.[3,4] The kinetics and extent of embrittlement are controlled by several mechanisms that depend on material parameters and aging temperature. Materials aged at 450°C show significant precipitation of phase-boundary carbides (also nitrides in high-nitrogen steels) and a large decrease in ferrite content of the material.[3,4] Such processes either do not occur or their kinetics are extremely slow at reactor temperatures. Consequently, data obtained at 450°C aging do not reflect reactor operating conditions, and extrapolation of the 450°C data to predict the extent of embrittlement at reactor temperatures is not valid. The chemical composition of the steel and the ferrite content and spacing are important parameters in controlling the extent and kinetics of embrittlement. Ferrite morphology strongly affects the extent of embrittlement, whereas material composition influences the kinetics of embrittlement. Small changes in the constituent elements of the cast material can cause the kinetics of embrittlement to vary significantly. The rate of embrittlement for a specific cast stainless steel is controlled by the kinetics of spinodal decomposition and the synergistic effects of carbide and G-phase precipitation. The activation energies for embrittlement can range from 65 to 230 kJ/mole. The influence of various precipitation processes on the kinetics of embrittlement is not well understood.

This paper presents an assessment of thermal aging embrittlement of cast stainless steels in LWR systems. Mechanical-property results from the present study and data from other investigations[9–14] have been analyzed to develop a procedure and preliminary correlations for predicting fracture toughness J-R curves of aged cast stainless steels from known material information. The present analysis has focussed on developing correlations for the fracture properties in terms of material information that can be determined from the certified material test record (CMTR) and on assuring that the correlations are adequately conservative for structurally "weak" materials. Fracture toughness of a specific cast stainless steel is estimates of the extent and kinetics of embrittlement. The extent of embrittlement is characterized by the room-temperature "normalized" Charpy-impact energy (i.e., Charpy impact energy per unit area). A correlation for the extent of embrittlement at "saturation", i.e., the minimum impact energy that can ever be achieved for the material after long-term aging, is given in terms of the chemical composition. The extent of embrittlement as a function of time and temperature of reactor service is then estimated from the extent of embrittlement at saturation and from the correlations describing the kinetics of embrittlement, which is also given in terms of the chemical composition. The fracture toughness J-R curve for the material is then obtained from correlation between room-temperature Charpy-impact energy which is used to characterize the extent of embrittlement and fracture toughness parameters. A common lower bound J-R curve for cast materials with unknown chemical composition is also defined.

2. Extent of Embrittlement

The Charpy-impact data obtained at room temperature indicate that for a specific heat of cast stainless steel, a saturation value of minimum impact energy is reached after aging for 3,000 - 10,000 h at 400°C or 30,000 - 60,000 h at 350°C. The variation of this saturation impact energy Cv_{sat} for different materials can be expressed in terms of a material parameter Φ which is determined from the chemical composition and ferrite morphology. It is well established that the extent of embrittlement increases with an increase in the ferrite content of the cast stainless steel. Furthermore, Charpy-impact data for several heats of CF-8 and CF-8M steels indicate that the impact energy decreases with an increase in the Cr content, irrespective of the ferrite content in the steel.[11] A better correlation is obtained when the total concentration of ferrite formers (i.e., Cr, Mo, and Si) is considered.[11] A sharp decrease in impact energy occurs when either the Cr content exceeds 18 wt.% or the concentration of Cr+Mo+Si exceeds 23.5 wt.%. An increase in the concentration of C or N in the steel also increases the extent of embrittlement because of the contribution to phase-boundary carbides or nitrides and the subsequent fracture by phase boundary separation.

Based on the amount of information available, two different methods for estimating the material parameter and saturation impact energy are presented. The first method utilizes only the information available in certified material test record (CMTR), i.e., chemical composition of the material. The second, more accurate, estimate of saturation impact energy can be obtained when metallographic information on ferrite morphology is also available, i.e., the measured values of ferrite content and mean ferrite spacing of the steel are known.

Method A – when only CMTR is available

The material parameter Φ can be estimated from the information available in CMTR, e.g., chemical composition. The ferrite content is calculated in terms of the Hull's equivalent factors

$$Cr_{eq} = Cr + 1.21(Mo) + 0.48(Si) - 4.99, \tag{1}$$

$$Ni_{eq} = (Ni) + 0.11(Mn) - 0.0086(Mn)^2 + 18.4(N) + 24.5(C) + 2.77, \tag{2}$$

where the chemical composition is in wt.%. The concentration of nitrogen is often not available in the CMTR; it is assumed to be 0.04 wt.% if not known. Thus, the ferrite content δ_c (in %) is given by

$$\delta_c = 100.3(Cr_{eq}/Ni_{eq})^2 - 170.72(Cr_{eq}/Ni_{eq}) + 74.22. \tag{3}$$

The measured and calculated values of ferrite content for the various heats used in studies at ANL[3,4], Framatome (FRA)[13], George Fischer Co. (GF)[9], Electricité de France (EdF)[11], Central Electricity Generation Board (CEGB)[12], and Electric Power Research Institute (EPRI)[15] are shown in Fig. 1. For most heats the difference between the estimated and measured values is within ±6% ferrite. The few heats for which the estimated ferrite contents are significantly lower than the measured values, in general, contain ≥10% nickel.

Different correlations are used for estimating the saturation impact energy of the various grades of cast stainless steel. For CF-3 and CF-8 steels, the material parameter Φ is expressed as

$$\Phi = \delta_c(\mathrm{Cr+Si})(\mathrm{C}+0.4\mathrm{N}), \tag{4}$$

and the saturation value of room-temperature impact energy, Cv_{sat} (in J/cm^2) is given by

$$\log_{10}Cv_{sat} = 1.15 + 1.374\exp(-0.0365\Phi). \tag{5}$$

The values of saturation room temperature impact energy predicted from Eqs. (4) and (5) and those observed experimentally for the studies at ANL, FRA, GF, EdF, CEGB, and EPRI are shown in Fig. 2. The curves shown in dash lines represent ±26% deviation from the predicted values. The difference between the predicted and observed values is <±15% for most of the materials.

A different expression for the material parameter is obtained for the Mo-bearing CF-8M steels. The material parameter Φ for CF-8M steels is given by

$$\Phi = \delta_c\mathrm{Cr}(\mathrm{C}+0.4\mathrm{N})(\mathrm{Ni+Si})^2/100, \tag{6}$$

and the saturation value of room-temperature impact energy, Cv_{sat}, is given by the relation

$$\log_{10}Cv_{sat} = 1.15 + 1.532\exp(-0.0467\Phi). \tag{7}$$

The nitrogen content is assumed to be 0.04 wt.% if not known. The observed room-temperature impact energy at saturation and values predicted from Eqs. (6) and (7) are shown in Fig. 3 for the data from ANL, FRA, GF, and EdF studies. The difference between observed and predicted values for the CF-8M steel is larger than that for the CF-3 or CF-8 steels. The curves shown by dash lines represent ±58% deviation from the predicted values.

Method B – when metallographic information is available

A more accurate estimate of saturation impact energy and a common expression for material parameter for the various grades of steel can be obtained when the measured values of ferrite content and mean ferrite spacing of the steel are known. In this case the material parameter Φ is representative of the structure as well as composition of the steel and is given by

$$\Phi = \delta_m^2(\mathrm{Cr+Mo+Si})(\mathrm{C}+0.4\mathrm{N})\mathrm{Ni}\lambda/10^4, \tag{8}$$

where δ_m is the measured ferrite content (in %) and λ is the mean ferrite spacing (in μm). The saturation value of room temperature impact energy, Cv_{sat}, is given by the relation

$$\log_{10}Cv_{sat} = 1.386 + 0.938\exp(-0.0205\Phi). \tag{9}$$

In the field, δ_m would have to be measured with a magne–gage or a ferrite scope (nonsaturation magnetic induction principle) and λ determined from metallographic replicas taken of the actual component. The nitrogen content is assumed to be 0.04 wt.% if not known.

Plots of room–temperature impact energy and material parameter Φ, calculated from Eqs. (8) and (9), are shown in Fig. 4. The data from studies at ANL, FRA, GF, CEGB, and EPRI are also shown in the figures. The curves shown in dash lines represent ±41% deviation from the predicted values. The saturation impact energies predicted from Eqs. (8) and (9) for CF–3 or CF–8 steels are comparable to those estimated from Eqs. (4) and (5), and for CF–8M steel are better than those estimated from Eqs. (6) and (7). The correlations expressed in Eqs. (4)–(7) do not consider the effects of Nb on embrittlement and, hence, may not be conservative for Nb–bearing cast stainless steels.

3. Kinetics of Embrittlement

The results from room-temperature Charpy-impact tests on the various experimental and commercial heats, aged up to 30,000 h at 290, 320, 350, 400, and 450°C, were analyzed to determine the kinetics of embrittlement. The variation of the Charpy-impact energy C_V (in daJ/cm^2) with time can be expressed as

$$\log_{10}C_V = \log_{10}C_{Vsat} + \beta\{1 - \tanh[(P - \theta)/\alpha]\}, \quad (10)$$

where C_{Vsat} (also in daJ/cm^2) is the saturation minimum impact energy reached after long-term aging, β is half the maximum change in $\log C_V$, θ is the log of the time to achieve β reduction in impact energy at 400°C, α is a shape factor, and P is the aging parameter defined by

$$P = \log_{10}[t] - \frac{Q}{19.143}\left\{\frac{1}{T_s+273} - \frac{1}{673}\right\}, \quad (11)$$

where Q is the activation energy (in J/mole) and t and T_s are the time (in h) and temperature (in °C) of aging. Equation (11) considers aging at 400°C as the baseline aging behavior for the material and parameter P is the log of the aging time at 400°C. The data obtained at 450°C aging are not representative of reactor operating conditions and, were therefore excluded from the analysis. Charpy data obtained after 290°C aging often showed no reduction in impact energy even after aging for 30,000 h; instead, a slight increase in impact energy was observed relative to the unaged material. The relatively short-time aging data at 290°C tend to bias the analyses to yield higher values of activation energies; therefore, the short-term aging results at 290°C were also excluded from the analysis for some of the heats. The values of the constants in Eqs. (10) and (11) are given in Table 2. The 95% confidence limits for activation energies are large for some heats because of the relatively small decrease in impact energy and large scatter in the data. Results from GF[9] and FRA[13] studies were also fitted to Eqs. (10) and (11) to obtain a consistent set of values for activation energy. The chemical composition and the constants in Eq. (10) and (11) for the GF and FRA heats are given in Table 3.

The constant β in Eq. (10) can be determined from the initial impact energy of the unaged material C_{Vint} and the saturation impact energy C_{Vsat}, i.e., $\beta = (\log C_{Vint} - \log C_{Vsat})/2$.

The results for the kinetics of embrittlement, Tables 2 and 3, indicate that the shape factor α increases linearly with Cv_{sat}. The best fit of the data for the various heats yields an expression

$$\alpha = 0.126 + 0.947 \log Cv_{sat}. \tag{12}$$

Thus, the constants β and α can be readily estimated from known information. Activation energy for the embrittlement process has been expressed in terms of the chemical composition of the cast material. The earliest correlation, proposed by Framatome, was based on the GF[9] data for 16 heats of cast stainless steel. Activation energy was expressed as a function of the concentrations (wt.%) of chromium, molybdenum, and silicon in the steel, thus

$$Q\ (\text{kJ/mole}) = -182.6 + 19.9\ \text{Si} + 11.08\ \text{Cr} + 14.4\ \text{Mo}. \tag{13}$$

The activation energy calculated from Eq. (13) for the process of embrittlement ranges from 65 to 105 kJ/mole for the various grades of cast stainless steel. However, the estimated activation energies for ANL or CEGB heats are a factor of 2 lower than the experimental values. The GF data set covers a relatively narrow range of compositions and the ferrite contents of most heats are above 30% and, therefore, is not representative of compositions defined by ASTM Specification A 351.

The correlations developed by ANL were based on a larger data base. Two separate correlations were proposed; one for the ANL[3,4] and FRA[13] data (15 heats), given by

$$\begin{aligned} Q\ (\text{kJ/mole}) = {} & 90.54 + 9.62\ \text{Cr} - 8.12\ \text{Ni} - 7.53\ \text{Mo} \\ & + 20.59\ \text{Si} - 123.0\ \text{Mn} + 317.7\ \text{N}, \end{aligned} \tag{14}$$

and the other for the GF[9] data (16 heats), given by

$$\begin{aligned} Q\ (\text{kJ/mole}) = {} & -66.65 + 6.90\ \text{Cr} - 5.44\ \text{Ni} + 8.08\ \text{Mo} \\ & + 17.15\ \text{Si} + 44.1\ \text{Mn} + 297.1\ \text{N}, \end{aligned} \tag{15}$$

where the constituent elements are given in wt.%. For a specific material composition, the activation energies predicted from Eqs. (13) and (15) are comparable, while those from Eq. (14) are higher. The ANL data used in developing the correlations represented only the high-temperature aging; the results for long-term aging (i.e., 30,000 h) at 290 or 320°C were not included in the analyses. Thus, the calculated activation energies primarily represent the kinetics of embrittlement at temperatures between 450 and 350°C. These values are 15 to 20% lower than those determined from aging data at temperatures between 400 and 290°C, Table 2.

The GF heats not only show very low activation energies for embrittlement, i.e., 65–105 kJ/mole, their aging behavior at 400°C is also significantly different than that for the ANL or FRA heats, Tables 2 and 3. The values of the constant θ in Eq. (10), which represent the log of the time for half the maximum change in impact energy at 400°C, are between 3.0 and 4.0 for the GF data set. These values are higher than those for the ANL or FRA heats, which range from 2.3 to 3.3. The constant θ for 12 of the 16 GF heats is >3.3. Such high values of θ are not observed for any other data set. The CEGB data[12] yield θ values of 2.3–2.6 and activation energies 185–215 kJ/mole. The aging behavior of recovery-annealed material from the KRB pump cover plate[4] is also consistent with ANL/FRA/CEGB data, viz., the constant θ is 2.3 and activation energy is ~180 kJ/mole. A low value of θ, i.e., 2.1, is also observed for the EPRI heat,[15] and limited data for the kinetics of embrittlement for the material* indicate a relatively high activation energy, ~230 kJ/mole. The low activation energies and high θ values are unique to the GF data set and most likely are due to the different initial heat treatment of the materials. In addition to the production heat treatment of 12 h at 1010 or 1050°C, the GF heats were annealed in the laboratory for 4 h at

---

* Unpublished work, Argonne National Laboratory.

1050°C and water quenched. GF Heat 280 was also tested in the production heat treatment condition, designated Heat 280N.[9] The effect of heat treatment is clearly reflected in the aging behavior of Heats 280 and 280N. The θ values for Heats 280 and 280N are 3.3 and 2.5, respectively. Activation energy for Heat 280N is ~20% higher than for Heat 280.[9] The kinetics data for the various data sets indicate that cast stainless steels with low activation energy for embrittlement, in general, have a high value of θ.

A mechanistic correlation based on the microstructural characteristics has also been proposed for estimating the activation energy for embrittlement regardless of the grade of material, range of chemical composition, fabrication process, and thermomechanical history of the material.[7,8] The activation energy for embrittlement is estimated from the volume fraction of G phase in the ferrite after aging the material for ~30,000 h at 400°C. Separate correlations are proposed for cast materials in which a large fraction of the ferrite/austenite boundaries are covered with carbides than for those without the phase boundary carbides. The premise being that the overall activation energy for embrittlement is controlled by the kinetics of spinodal decomposition and the synergistic effects of G–phase precipitation in ferrite and carbide precipitation at phase boundaries. Spinodal decomposition is slower for materials which show significant G–phase precipitation or Ni–Si clustering, since Ni is depleted from the ferrite matrix. Such effects are more pronounced at 400°C aging, thus, the activation energy of embrittlement is smaller than the ~230 kJ/mole value associated with spinodal decomposition in binary Fe–Cr alloys. A schematic representation of the model is shown in Fig. 5. The lines correspond to the aging time at different temperatures to achieve half the maximum decrease in Charpy impact energy for three hypothetical cases of metallurgical transformation. Kinetics of embrittlement controlled only by spinodal decomposition are represented by solid line. Activation energy is decreased when G–phase precipitation and Ni–Si clustering accompany spinodal decomposition, shown by chain–dash line. Precipitation of phase boundary carbides increase the activation energy as represented by the dash line.

The data on the kinetics of embrittlement of cast stainless steels are in general agreement with this model, i.e., cast materials with significant G–phase precipitation show low activation energies of embrittlement. Furthermore, in Fig. 5 the log of the time at 400°C represents the constant θ in Eq. (10). The model indicates that θ should be high for cast materials which show low activation energy for embrittlement. The GF, FRA, ANL, and CEGB data sets are consistent with this behavior. The GF data set with low activation energies and high θ values corresponds to the chain dash line, CEGB data set with high activation energies and low θ values corresponds to the solid line , and the FRA and ANL data sets fall in between the two cases. Also, the GF heats show significant G–phase precipitation, ANL heats show some, and no G–phase is observed for the CEGB heats.

The factors that promote G–phase precipitation and the exact nature of the interactions, if any, between G phase and spinodal decomposition are not well understood. According to the microstructure–based model a high Si content promotes G–phase precipitation and Ni–Si clustering, and therefore leads to low activation energy.[7] Figure 5 indicates that this should also result in higher values of θ. Table 3 shows that GF Heats 281, 282, 283, 284, and 287 contain <0.5 wt.% Si while the others contain >1.3 wt.% Si. Since the casting process and heat treatment are essentially the same for these heats, the low–Si heats should yield higher activation energies and low values of θ. In all cases, θ values are higher for the low–Si heats and activation energies are not significantly different than those for the high–Si heats. Similar inconsistencies are observed for the ANL and FRA data sets.

The model also stipulates that depletion of Ni from the ferrite matrix due to G–phase precipitation slows spinodal decomposition. The activation energy is low because G–phase precipitation is more pronounced at 400°C than that at lower temperatures. The kinetics of reembrittlement of recovery-annealed materials are not consistent with this behavior.§ Annealing of fully embrittled material for 1 h at 55°C and water quenching, dissolves the α' precipitates while the G–phase is not affected. Thus, thermal aging of the material should yield high values of activation energy since G phase precipitates are already present in the matrix. Experimental results for CF–3, CF–8, and CF–8M steels indicate that the kinetics of embrittlement of recovery–annealed material are identical to that for the as–cast material. These results suggest that the activation energy for embrittlement is not effected by differences in G–phase precipitation at different aging temperatures.

Charpy data for the kinetics of embrittlement were reanalyzed to develop a general correlation for activation energy which would be applicable for all chemical compositions within the ASTM Specification A 351 and valid for the entire temperature range of extrapolation, i.e., 400 to 280°C. Activation energy for embrittlement was expressed in terms of the chemical composition as well as the constant θ to incorporate the effects of heat treatment and the casting process, on the kinetics of embrittlement. The best fit of the data from ANL, FRA, GF, and CEGB studies (36 heats) yield an expression given by

$$Q\ (\text{kJ/mole}) = 10\ \Big[74.06 - (7.66 - 0.46\ I_1)\ \theta - 4.35\ \text{Si} + 1.38\ I_2\ \text{Mo} - 1.67\ \text{Cr} - (2.22 + 3.56\ I_1)\ \text{Mn} + (108.8 - 75.3\ I_1)\ \text{N}\Big], \quad (16)$$

where the indicators $I_1 = 0$ and $I_2 = 1$ for CF–3 or CF–8 steels and assume the values of 1 and 0, respectively, for CF–8M steels. The estimated and observed values of Q for the ANL,

---

§ Unpublished work, Argonne National Laboratory.

FRA, CEGB, and GF heats are plotted in Fig. 6. The error bars represent 95% confidence limits for the observed values of Q. The dashed lines represent ±20% range. The predicted values are within the 95% confidence limits for all the heats. Equation (16) is applicable for compositions within the ASTM Specification A 351 with a 1.2 wt.% maximum for Mn content. Furthermore, the values of Q predicted from Eq. (15) should be between 65 kJ/mole minimum and 250 kJ/mole maximum; Q is assumed to be 65 kJ/mole if the predicted values are lower, and 250 kJ/mole if the predicted values are higher.

4. Estimation of Impact Energy

The room temperature Charpy impact energy of a specific cast stainless steel can be estimated from the correlations presented in Sections 2 and 3. The impact energy at saturation Cv_{sat} is determined from the chemical composition of the cast material. The saturation value represents the minimum impact energy that would ever be achieved by the material after long term aging. Estimation of the decrease in impact energy as a function of time and temperature of service requires additional information, namely, the initial impact energy of the unaged material and the aging behavior at 400°C, i.e., the value of constant θ.

The estimated and observed impact energies for some of the ANL, FRA, and GF heats aged at temperatures between 300 and 350°C, are shown in Figs. 7 and 8. For each heat, first, the impact energy at saturation was determined from Eqs. (1) – (7), i.e., Method A. The activation energy for embrittlement was obtained from Eq. (16); observed values of θ were used for all the heats. Then the change in impact energy with time and temperature of aging was estimated from Eqs. (10) and (11). The shape factor α in Eq. (10) is obtained from Eq. (12) and the constant β is determined from the initial and saturation values of impact energy. The estimated change in impact energy shows good agreement with the observed aging behavior for most of the heats. The shape factor estimated from Eq. (12) is low for a few heats, e.g., Heat 286. Thus, the predicted decrease in impact energy is slower than that observed. For some heats, the estimated Cv_{sat} is higher than the observed value, e.g., Heats P4 and B. Such discrepancies are caused by underestimation of the ferrite content of the steel. As mentioned earlier, the ferrite contents estimated from Eqs. (1) – (3) for heats containing ≥10 wt.% Ni, are always lower than the measured values. A more accurate estimate of Cv_{sat} can be obtained from Eqs. (8) and (9). A nonconservative value for Cv_{sat} can also be avoided by using the lower limit expressions for Eqs. (5) and (7), i.e., the lower bound curve shown by dashed line in Figs (2) and (3).

The values of θ are not available for cast stainless steel components in the field, and can only be obtained from aging archive material for 5,000 to 10,000 h at 400°C. Fortunately parametric studies show that the aging response at reactor temperatures is relatively insensitive to the values of θ. Impact energies estimated from actual and assumed values of θ are shown in Fig. 9 for four heats. Varying θ between 2.3 and 3.3 has an almost identical aging behavior at 300°C. At 320°C, a low value of θ predicts slightly faster kinetics. The reverse is true at 280°C (not shown in Fig. 9), i.e., a low value of θ predicts slower kinetics. However, the differences in the estimated aging behavior at 280 or 320°C for values in the range of interest are minimal, and a median value of 2.9 for θ can be used to estimate embrittlement at reactor temperatures. Charpy impact tests have been conducted on reactor-aged components from the Shippingport reactor to benchmark the laboratory data and validate these correlations; the results are presented in a companion paper.†

---

† "Studies of Aged Cast Stainless Steel from Shippingport Reactor," this conference.

5. Fracture Toughness

Estimation of J–R Curves

Thermal aging of cast stainless steels decreases their fracture toughness at room temperature as well as at reactor temperatures, i.e., 280–320°C. The fracture toughness results are consistent with the Charpy impact data, i.e., unaged and aged materials that show low impact strength also exhibit lower fracture toughness. The fracture toughness J–R curve for a specific cast stainless steel can be estimated from its room–temperature impact energy. The J–R curve is expressed by power-law relation $J_d = C\Delta a^n$, where J_d is deformation J(in kJ/m^2) as per ASTM Specifications E 813–85 and E 1152, Δa is the crack extension (in mm), and C and n are constants. The coefficient C at room and reactor temperatures and the room–temperature Charpy impact energy for aged and unaged cast stainless steels are plotted in Fig. 10. Fracture toughness data from ANL,[3,4] FRA,[14] and EPRI[15] studies are included in the figure. At both temperatures, the coefficient C decreases with a decrease in impact energy. Separate correlations are obtained for CF–3 or CF–8 steels and for CF–8M steel, the latter show a larger decrease in fracture toughness for a given impact energy. Thus, the J–R curve at room temperature for CF–3 and CF–8 steels is given by

$$J_d = 37.5[C_{Vsat}]^{0.52}[\Delta a]^{0.60}, \qquad (17)$$

and for CF–8M steel by

$$J_d = 8.2[C_{Vsat}]^{0.85}[\Delta a]^{0.50}. \qquad (18)$$

At temperatures between 290 and 320°C, the J–R curve for CF–3 and CF–8 steels is given by

$$J_d = 48.5[C_{Vsat}]^{0.45}[\Delta a]^{0.45}, \qquad (19)$$

and for CF–8M steel by

$$J_d = 34.3[C_{Vsat}]^{0.52}[\Delta a]^{0.45}. \qquad (20)$$

In Eqs. (17)–(20), J_d is expressed in kJ/m^2, C_V in J/cm^2, and Δa in mm. The lower-bound curves (shown in chain–dash lines in Fig. 10) are used for CF–3 and CF–8 steels to assure that the estimated J–R curve is conservative for all material and aging conditions. The exponent of Δa, i.e., 0.60, 0.50, and 0.45 in Eqs. (17)–(20) represents the average value determined from the experimental J–R curve data for a given material specification and temperature, Fig. 11. Fracture toughness data at 290°C on long-term-aged material are sparse. J–R curve tests at 290°C are in progress on several heats of cast stainless steels aged for 30,000 h at 290, 320, and 350°C. The results will be used to optimize and validate the correlations. The limited data available[14] indicate that J values at any other intermediate temperature can be linearly interpolated from the values at room temperature and at 290°C.

The fracture toughness J–R curve for a specific material and aging condition can be obtained from the correlations expressed in Eqs. (17)–(20) and the procedure for estimating room-temperature impact energy described in Section 4. Comparisons of the experimental J_d values at 0.5-, 1.0-, 2.5-, and 5.0-mm-crack extension and those estimated using Method A to determine room temperature impact energy for various partially and fully aged cast stainless steels, are shown in Figs. 12 and 13. The estimated J_d values are always lower but within ~50% of the experimental values of J_d. Examples of the experimental and estimated J–R curve at saturation, i.e., the minimum fracture toughness that would ever be achieved for the material, are shown in Figs. 14 and 15. Examples of the experimental estimated J–R curves for several partially aged cast stainless steels are shown in Figs. 16. These results may be compared with the saturation J–R curves for the materials, Figs. 14 and 15, and the J–R curves for the unaged materials, Fig. 17. The measured room-temperature Charpy impact energy was used to estimate the curves in Fig. 17. The estimated J–R curves show good agreement with the experimental results for most of the heats and are essentially conservative.

Lower-bound J-R Curves

For cast stainless steels of unknown chemical composition, a lower-bound fracture toughness is defined for a given material specification and temperature. Equations (5) and (7) indicate that for cast stainless steels within the ASTM Specification A 351, the saturation room-temperature impact energy can be as low as 25 J/cm^2 for CF-3 and CF-8 steels and 20 J/cm^2 for CF-8M steel. Thus, from Eqs. (17)-(20), a lower-bound fracture toughness J-R curve at room temperature for CF-3 and CF-8 steels is given by

$$J_d = 200.0[\Delta a]^{0.60}, \qquad (21)$$

and for CF-8M steel by

$$J_d = 104.6[\Delta a]^{0.50}. \qquad (22)$$

At 290 to 320°C a lower-bound fracture toughness J-R curve for CF-3 and CF-8 steels is given by

$$J_d = 206.5[\Delta a]^{0.45}, \qquad (23)$$

and for CF-8M steel by

$$J_d = 162.9[\Delta a]^{0.45}. \qquad (24)$$

The J-R curves predicted from Eqs. (21)-(24) are shown in Fig. 18. The cast stainless steels used in U. S. nuclear industry generally have <15% ferrite. The lower bound J-R curves represented by Eqs. (21)-(24) are based on the "worst case" chemical composition, >20% ferrite, and structurally weak cast stainless steels and, thus, are very conservative for most steels. Less conservative estimates of lower bound J-R curves can be obtained if the ferrite content of the steel is known. The ferrite content of a cast stainless steel component can be measured in the field with a ferrite scope using a remote probe. The values of material parameter Φ in Eqs. (4) and (6) can be scaled with respect to the ferrite content to obtain more realistic estimates of saturation Charpy impact energy and J-R curves for the material.

Procedure for Estimating Fracture Toughness

A flow diagram of the sequential steps required for estimating fracture toughness J-R curves is shown in Fig. 19. In Section A, "lower-bound" fracture toughness J-R curve for cast stainless steels of unknown chemical composition are defined. Sections B and C present procedures for estimating J–R curves when some information is known about the material, e.g., CMTR is available. Section B describes the estimation of "saturation" J–R curves, i.e., the lowest toughness that would ever be achieved for the material after long-term service. Estimation of "service time" J–R curves, i.e., fracture toughness at any given time and temperature of service, is described in Section C. The service time J–R curves depend on the kinetics of embrittlement, i.e., the rate of decrease of fracture toughness as a function of reactor–service time.

6. Conclusion

A procedure and correlations are presented for predicting fracture toughness J–R curves and impact strength of aged cast stainless steels from known material information. Fracture toughness of a specific cast stainless steel is estimated from the extent and kinetics of embrittlement. Embrittlement of cast stainless steels is characterized in terms of room–temperature Charpy–impact energy. The extent or degree of embrittlement at "saturation", i.e., the minimum impact energy that can ever be achieved for the material after long–term aging, is described in terms of a material parameter Φ, which is determined from the chemical composition and ferrite morphology. The room–temperature impact energy as a function of time and temperature of reactor service is estimated from the kinetics of embrittlement, which are also determined from the chemical composition. The fracture toughness J–R curve for the material is then obtained from correlations between room–temperature Charpy–impact energy and fracture toughness parameters. A common "lower–bound" J–R curve for cast stainless steels with unknown chemical composition is also defined. Examples for estimating impact strength and fracture toughness of cast stainless steel components during reactor service are described. Estimated fracture toughness J–R curves show good agreement with the experimental results for most of the cast materials and are conservative for structurally "strong" materials.

Mechanical–property tests are being conducted on long–term–aged materials as well as reactor–aged components to benchmark the laboratory data and validate the correlations. The correlations will be optimized with respect to casting process and macrostucture of the steel since the toughness of centrifugally cast steels is generally higher than that of static cast steels. Correlations are also being developed to estimate the flow stress of service–aged cast stainless steels. At present, fracture toughness analyses of cast components are based on the tensile properties of unaged material. This gives conservative estimates of applied J for load control situations. Typically, thermal aging increases the flow stress by 25 to 30% for materials that are sensitive to aging.

Acknowledgements

This work was supported by the Office of the Nuclear Regulatory Research in the U. S. Nuclear Regulatory Commission. The author is grateful to A. Sather, G. M. Dragel, L. Y. Bush, T. M. Galvin, and W. F. Burke for experimental contributions. The author also wishes to thank J. Muscara, W. J. Shack, and T. F. Kassner for their helpful discussions.

References

1. O. K. Chopra and H. M. Chung, "Aging Degradation of Cast Stainless Steels: Effects on Mechanical Properties," in *Environmental Degradation of Materials in Nuclear Power Systems–Water Reactors*, eds. G. J. Theus and J. R. Weeks, The Metallurgical Society, Warrendale, PA., pp. 737–748 (1988).

2. O. K. Chopra and H. M. Chung, "Effect of Low-Temperature Aging on the Mechanical Properties of Cast Stainless Steels," in *Properties of Stainless Steels in Elevated Temperature Service*, M. Prager, ed., MPC-Vol. 26, PVP-Vol. 132, American Society of Mechanical Engineers, New York, pp. 79-105 (1988).

3. O. K. Chopra, "Thermal Aging of Cast Stainless Steels: Mechanisms and Predictions," in *Fatigue, Degradation, and Fracture - 1990*, W. H. Bamford, C. Becht, S. Bhandari, J. D. Gilman, L. A. James, and M. Prager, eds., PVP - Vol. 195, MPC - Vol. 30, American Society of Mechanical Engineers, New York, pp. 193-214 (1990).

4. O. K. Chopra and A. Sather, *Initial Assessment of the Mechanisms and Significance of Low-Temperature Embrittlement of Cast Stainless Steels in LWR Systems*, NUREG/CR-5385, ANL-89/17 (August 1990).

5. H. M. Chung and O. K. Chopra, "Kinetics and Mechanism of Thermal Aging Embrittlement of Duplex Stainless Steels," in *Environmental Degradation of Materials in Nuclear Power Systems-Water Reactors*, Proc. Third Intl. Symp., Traverse City, MI, August 30-September 3, 1987, G. J. Theus and J. R. Weeks, eds., The Metallurgical Society, Warrendale, PA, pp. 359-370 (1988).

6. H. M. Chung and O. K. Chopra, "Long-Term Aging Embrittlement of Cast Austenitic Stainless Steels - Mechanism and Kinetics," in *Properties of Stainless Steels in Elevated Temperature Service*, M. Prager, ed., MPC-Vol. 26, PVP-Vol. 132, ASME, New York, 1988, pp. 17-34.

7. H. M. Chung, "Thermal Aging of Decommissioned Reactor Cast Stainless Steel Components and Methodology for Life Prediction," in *Life Assessment and Life Extension of Power Plant Components*, T. V. Narayanan, C. B. Bond, J. Sinnappan, A. E. Meligi, M.

Prager, T. R. Mager, J. D. Parker, and K. Means, eds., PVP-Vol. 171, ASME, New York, 1989, pp. 111–125.

8. H. M. Chung and T. R. Leax, "Embrittlement of Laboratory and Reactor Aged CF3, CF8, and CF8M Duplex Stainless Steels," *Mater. Sci. and Tech.* **6**, 249–262 (1990).

9. A. Trautwein, and W. Gysel, "Influence of Long Time Aging of CF-8 and CF-8M Cast Steel at Temperatures Between 300 and 500°C on the Impact Toughness and the Structure Properties," in *Stainless Steel Castings*, V. G. Behal and A. S. Melilli, eds., ASTM STP 756, pp. 165–189 (1982).

10. E. I. Landerman, and W. H. Bamford, "Fracture Toughness and Fatigue Characteristics of Centrifugally Cast Type 316 Stainless Steel Pipe after Simulated Thermal Service Conditions," in *Ductility and Toughness Considerations in Elevated Temperature Service*, ASME MPC-8, pp. 99–127 (1978).

11. S. Bonnet, J. Bourgoin, J. Champredonde, D. Guttmann, and M. Guttmann, "Relationship between Evolution of Mechanical Properties of Various Cast Duplex Stainless Steels and Metallurgical and Aging Parameters: An Outline of Current EDF Programmes," *Mater. Sci. and Technol.*, **6**, 221–229 (1990).

12. P. H. Pumphrey and K. N. Akhurst, "Aging Kinetics of CF3 Cast Stainless Steel in Temperature Range 300 – 400°C," *Mater. Sci. and Technol.*, **6**, 211–219 (1990).

13. G. Slama, P. Petrequin, and T. Mager, "Effect of Aging on Mechanical Properties of Austenitic Stainless Steel Castings and Welds," presented at *SMIRT Post-Conference Seminar 6, Assuring Structural Integrity of Steel Reactor Pressure Boundary Components*, August 29–30, 1983, Monterey, Calif.

14. Y. Meyzaud, P. Ould, P. Balladon, M. Bethmont, and P. Soulat, "Tearing Resistance of Aged Cast Austenitic Stainless Steel," presented at *Intl. Conf. on Thermal Reactor Safety (NUCSAFE 88)*, October 1988, Avignon, France.

15. P. McConnell and J. W. Sheckherd, *Fracture Toughness Characterization of Thermally Embrittled Cast Duplex Stainless Steel*, Report NP-5439, September 1987, Electric Power Research Institute, Palo Alto, Calif.

Table 1. *Product Form, Chemical Analysis, Hardness and Ferrite Morphology of Cast Stainless Steel*

				Composition (wt.%)									Ferrite[a] (%)			λ
Heat	Grade	Product	Size (mm)	Mn	Si	P	S	Mo	Cr	Ni	N	C	Calc.	Meas.	R_B	(μm)
47	CF-3	Keel B.	180 x 120 x 30-90	0.60	1.06	0.007	0.006	0.59	19.81	10.63	0.028	0.018	8.4	16.3	79.7	68
52	CF-3	Keel B.	180 x 120 x 30-90	0.57	0.92	0.012	0.005	0.35	19.49	9.40	0.052	0.009	10.3	13.5	81.6	69
51	CF-3	Keel B.	180 x 120 x 30-90	0.63	0.86	0.014	0.005	0.32	20.13	9.06	0.058	0.010	14.3	18.0	83.8	52
56	CF-8	Keel B.	180 x 120 x 30-90	0.57	1.05	0.007	0.007	0.34	19.65	9.28	0.030	0.066	7.3	10.1	82.5	84
59	CF-8	Keel B.	180 x 120 x 30-90	0.60	1.08	0.008	0.007	0.32	20.33	9.34	0.045	0.062	8.8	3.5	83.2	75
61	CF-8	Keel B.	180 x 120 x 30-90	0.65	1.01	0.007	0.007	0.32	20.65	8.86	0.080	0.054	10.0	13.1	85.3	82
60	CF-8	Keel B.	180 x 120 x 30-90	0.67	0.95	0.008	0.006	0.31	21.05	8.34	0.058	0.064	15.4	21.1	86.7	63
63	CF-8M	Keel B.	180 x 120 x 30-90	0.61	0.58	0.007	0.006	2.57	19.37	11.85	0.031	0.055	6.4	10.4	81.6	81
66	CF-8M	Keel B.	180 x 120 x 30-90	0.60	0.49	0.012	0.007	2.39	19.45	9.28	0.029	0.047	19.6	19.8	85.3	41
65	CF-8M	Keel B.	180 x 120 x 30-90	0.50	0.48	0.012	0.007	2.57	20.78	9.63	0.064	0.049	20.9	23.4	89.0	43
64	CF-8M	Keel B.	180 x 120 x 30-90	0.60	0.63	0.006	0.005	2.46	20.76	9.40	0.038	0.038	29.0	28.4	89.7	41
69	CF-3	Slab	610 x 610 x 76	0.63	1.13	0.015	0.005	0.34	20.18	8.59	0.028	0.023	21.0	23.6	83.7	35
68	CF-8	Slab	610 x 610 x 76	0.64	1.07	0.021	0.014	0.31	20.64	8.08	0.062	0.063	14.9	23.4	84.6	87
74	CF-8M	Slab	610 x 610 x 76	0.54	0.73	0.022	0.016	2.51	19.11	9.03	0.048	0.064	15.5	18.4	85.8	90
75	CF-8M	Slab	610 x 610 x 76	0.53	0.67	0.022	0.012	2.58	20.86	9.12	0.052	0.065	24.8	27.8	89.5	69
P2	CF-3	Pipe	930 OD 73 Wall	0.74	0.94	0.019	0.006	0.16	20.20	9.38	0.040	0.019	12.5	15.6	83.8	69
I	CF-3	Impeller	660 dia	0.47	0.83	0.030	0.011	0.45	20.20	8.70	0.032	0.019	20.4	17.1	81.0	65
P1	CF-8	Pipe	890 OD 63 Wall	0.59	1.12	0.026	0.013	0.04	20.49	8.10	0.056	0.036	17.7	24.1	84.9	90
P4	CF-8M	Pipe	580 OD 32 Wall	1.07	1.02	0.019	0.015	2.05	19.64	10.00	0.151	0.040	5.9	10.0	83.1	182
KRB	CF-8	Pump Cover	890 dia	0.31	1.1	-	-	0.17	21.99	8.03	0.038	0.062	27.7	34.0	-	-

[a] Calculated from the composition with Hulls equivalent factor
Measured by ferrite scope AUTO Test FE, Probe Type FSP-1

Table 2. Activation Energies for the Kinetics of Embrittlement for Cast Stainless Steels

Heat	Parameter Φ[a]	Cv_{sat} (J/cm^2)	Constants β	θ	α	Q [kJ/mole (kcal/mole)] Average	95% Confidence Limit
47	12.0	174.2	0.063	2.35	1.40	187 (44.7)	73–300 (17.5–71.8) [c]
51	10.8	149.2	0.083	3.00	0.76	221 (52.8)	123–320 (29.3–76.4) [c]
69	12.4	96.9	0.202	3.05	0.93	167 (40.0)	120–215 (28.7–51.3) [c]
59	22.2	99.8	0.166	3.12	1.40	229 (54.7)	156–301 (37.4–72.0)
60	45.5	52.0	0.288	2.95	0.89	227 (54.2)	186–267 (44.4–63.9)
68	74.4	46.4	0.348	3.00	0.74	169 (40.5)	136–204 (32.4–48.2)
P1	53.5	58.7	0.282	2.38	0.75	249 (59.6)	210–289 (50.2–69.1)
63	15.8	111.7	0.155	3.20	1.40	119 (28.4)	67–170 (16.0–40.7)
64	39.4	45.2	0.304	2.75	0.62	156 (37.4)	131–181 (31.4–43.2)
65	40.3	58.5	0.269	2.93	0.94	191 (45.7)	154–228 (36.8–54.6)
66	19.5	106.3	0.149	3.02	1.30	203 (48.4)	125–280 (29.9–66.9) [c]
75	106.4	34.7	0.422	2.76	0.53	146 (34.8)	127–165 (30.3–39.4)
P4	41.5	53.8	0.325	2.95	0.89	143 (34.2)	115–171 (27.6–40.8)

[a] Calculated from Eq. (8).

[b] Standard deviation is large because of the relatively small decrease in impact energy and a large scatter in data.

Table 3. Chemical Composition and the Kinetics of Embrittlement for George Fischer and Framatome Heats of Cast Stainless Steels

Heat	Chemical Composition (wt.%) Cr	Mo	Si	Ni	Mn	C	N	Cv_{sat} (J/cm^2)	Constants β	θ	α	Q [kJ/mole ((kcal/mole)]
277	20.5	0.06	1.81	8.13	0.54	0.052	0.019	33.5	0.488	3.65	0.55	88 (21.0)
278	20.2	0.13	1.00	8.27	0.28	0.038	0.030	68.3	0.381	4.05	0.47	63 (15.0)
279	22.0	0.22	1.36	7.85	0.37	0.040	0.032	23.8	0.586	3.21	0.69	92 (21.9)
280	21.6	0.25	1.37	8.00	0.50	0.028	0.038	24.4	0.591	3.30	0.73	87 (20.7)
281	23.1	0.17	0.45	8.60	0.41	0.036	0.053	26.6	0.560	3.76	0.42	93 (22.1)
282	22.5	0.15	0.35	8.53	0.43	0.035	0.040	30.0	0.525	3.73	0.43	98 (23.4)
283	22.6	0.23	0.53	7.88	0.48	0.036	0.032	23.8	0.580	3.65	0.43	83 (19.8)
284	23.0	0.17	0.52	8.23	0.28	0.025	0.037	23.8	0.560	3.71	0.41	87 (20.9)
291	19.6	0.66	1.59	10.60	0.28	0.065	0.054	121.9	0.235	3.89	0.79	77 (18.5)
292	21.6	0.13	1.57	7.52	0.34	0.090	0.039	22.2	0.392	3.08	0.46	99 (23.7)
285	18.8	2.35	0.86	9.49	0.48	0.047	0.039	64.3	0.347	3.76	0.34	82 (19.6)
286	20.2	2.44	1.33	9.13	0.40	0.072	0.062	20.5	0.571	3.11	0.62	106 (25.2)
287	20.5	2.58	0.51	8.46	0.50	0.047	0.033	23.8	0.563	3.52	0.42	92 (21.9)
288	19.6	2.53	1.70	8.40	0.47	0.052	0.022	19.4	0.643	3.02	0.64	106 (25.3)
289	19.7	2.30	1.44	8.25	0.48	0.091	0.032	21.1	0.571	3.32	0.39	90 (21.6)
290	20.0	2.40	1.51	8.30	0.41	0.054	0.050	21.1	0.602	3.49	0.11	81 (19.3)
C	20.7	0.13	1.09	8.19	1.09	0.042	0.035	51.0	0.393	3.30	0.45	83 (19.9)
E	21.0	0.08	0.54	8.47	0.80	0.035	0.051	45.0	0.334	2.63	0.65	133 (31.8)
F	19.7	0.34	1.16	8.33	0.26	0.038	0.026	83.0	0.282	2.45	1.23	176 (41.1)
B	20.1	2.52	0.93	10.56	0.83	0.053	0.042	31.0	0.478	2.55	0.47	129 (30.7)
D	19.2	2.44	0.94	10.32	1.12	0.026	0.063	33.0	0.439	3.30	0.40	90 (21.4)

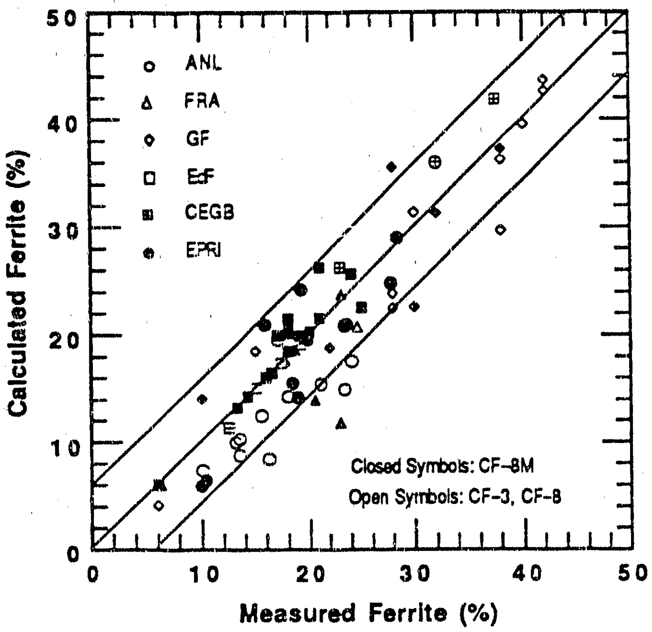

Figure 1. Measured and Calculated Ferrite Contents for Various Heats of Cast Stainless Steel.

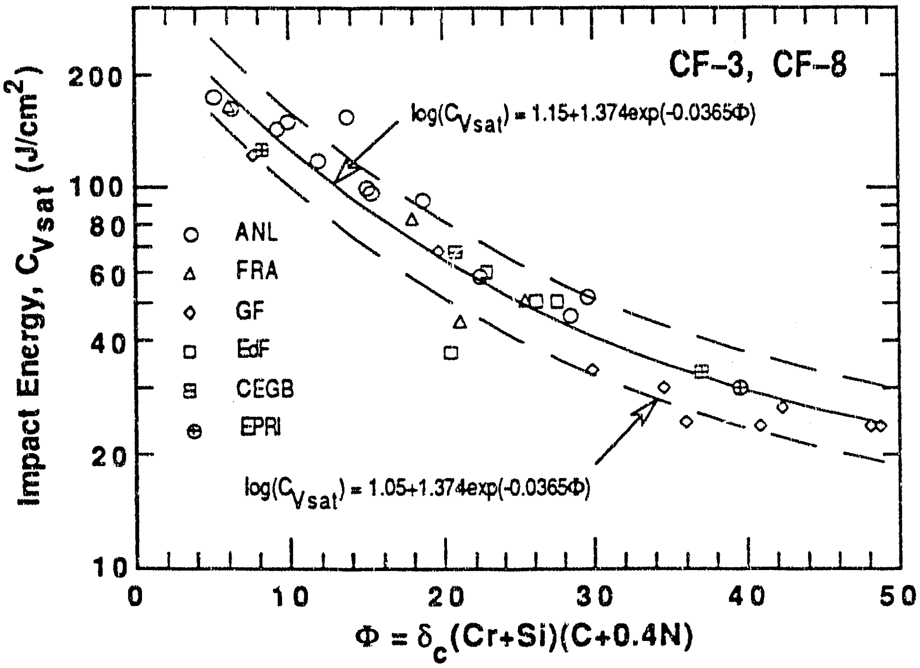

Figure 2. Correlation between Room Temperature normalized Charpy-impact Energy at Saturation and Material Parameter Φ (Method A) for CF-3 and CF-8 Steels.

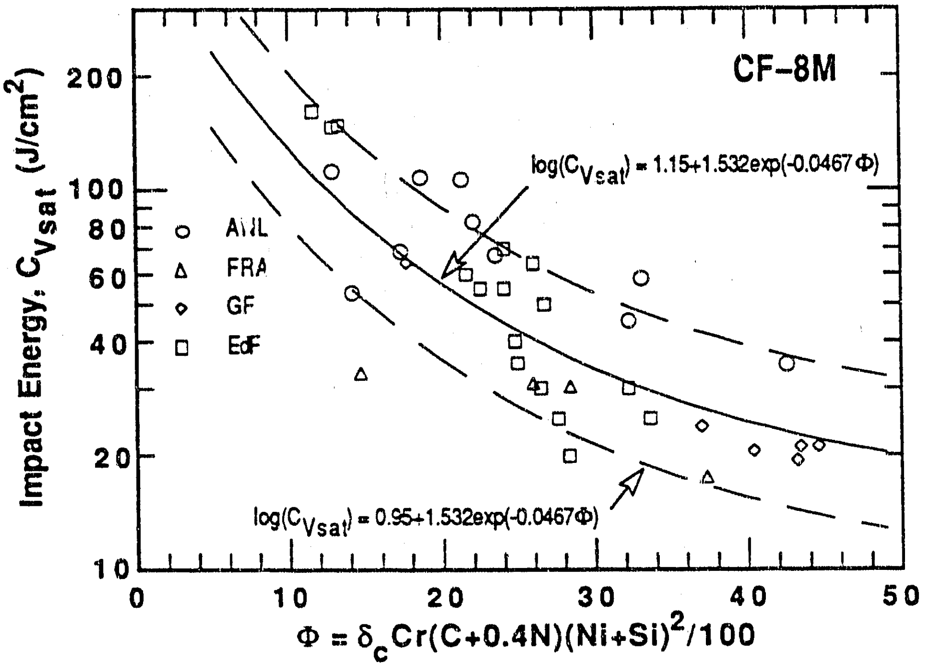

Figure 3. *Correlation between Room Temperature normalized Charpy-impact Energy at Saturation and Material Parameter Φ (Method A) for CF-8M Steel.*

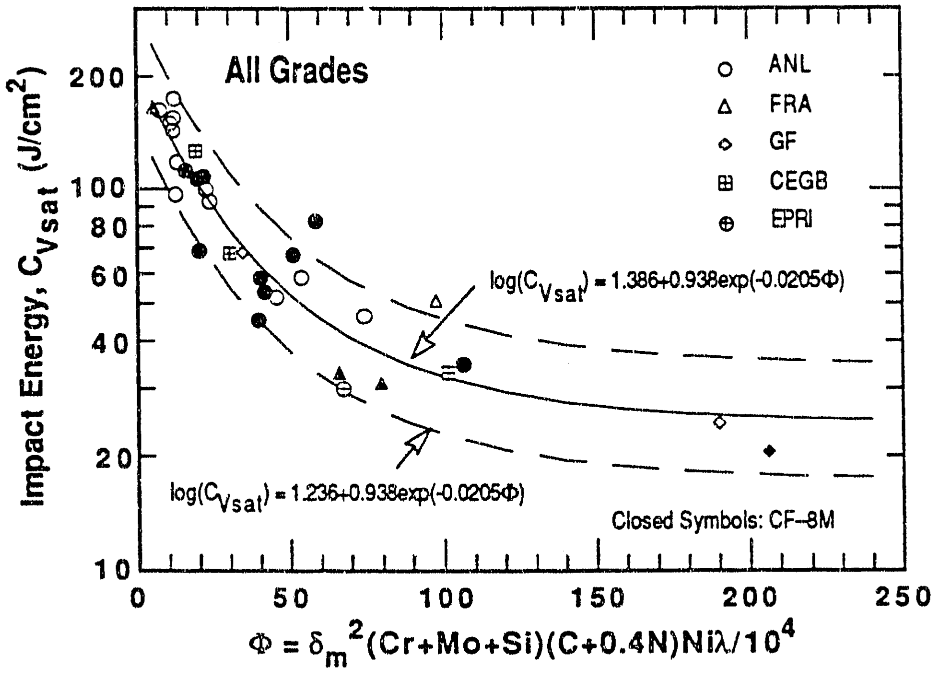

Figure 4. *Correlation between Room Temperature normalized Charpy-impact Energy at Saturation and Material Parameter Φ (Method B) for All Grades of Cast Stainless Steel.*

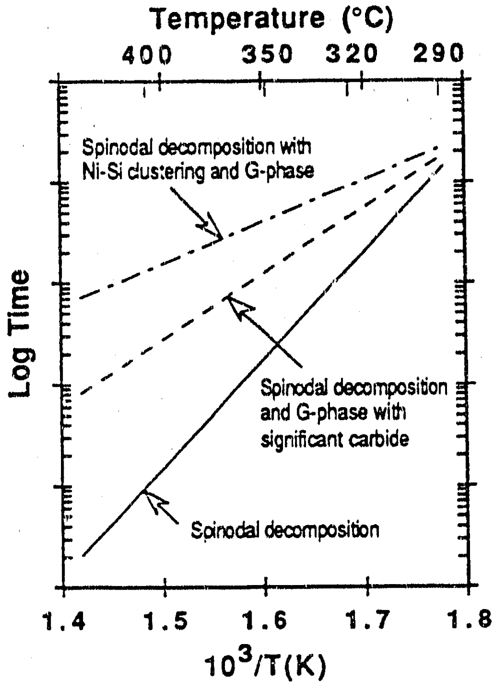

Figure 5. *Schematic Illustration of the Kinetics of Embrittlement of Cast Stainless Steels.*

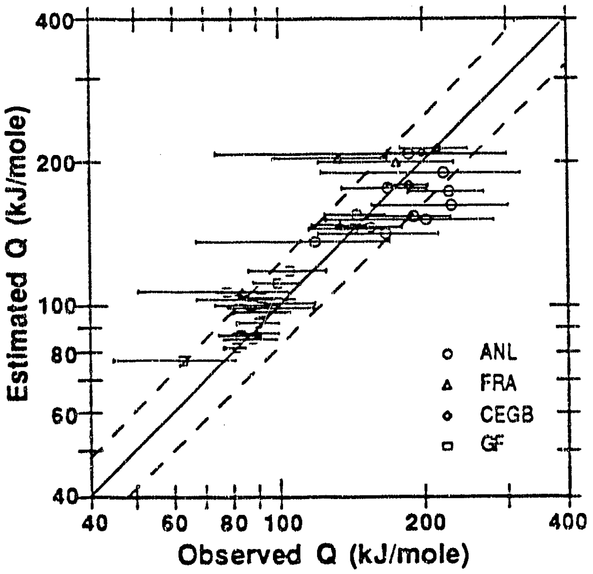

Figure 6. *Observed and Estimated Activation Energy for Embrittlement of Cast Stainless Steels.*

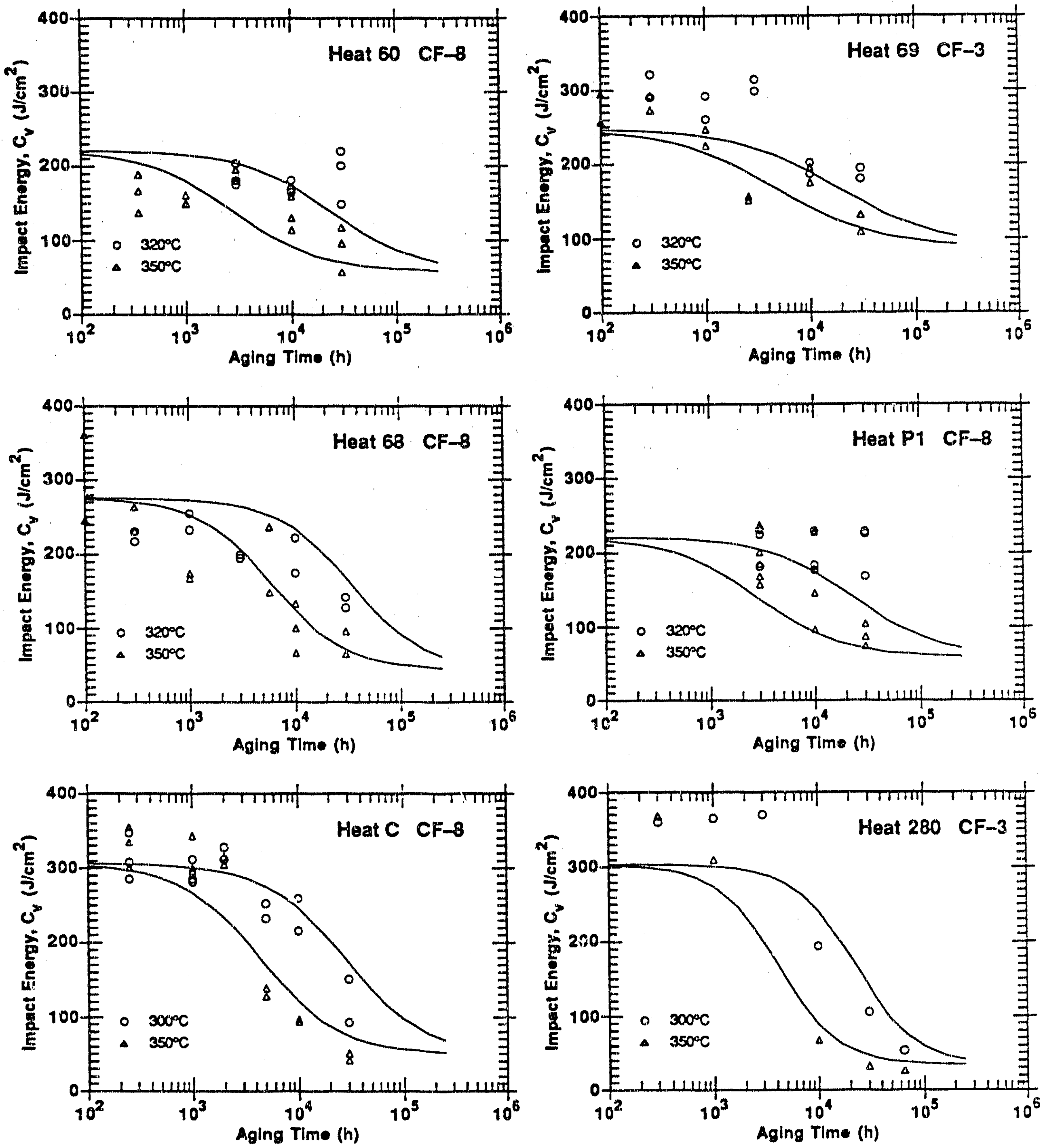

Figure 7. Observed and Estimated Room-Temperature Charpy Impact Energy for Aged CF-3 and CF-8 Cast Stainless Steels.

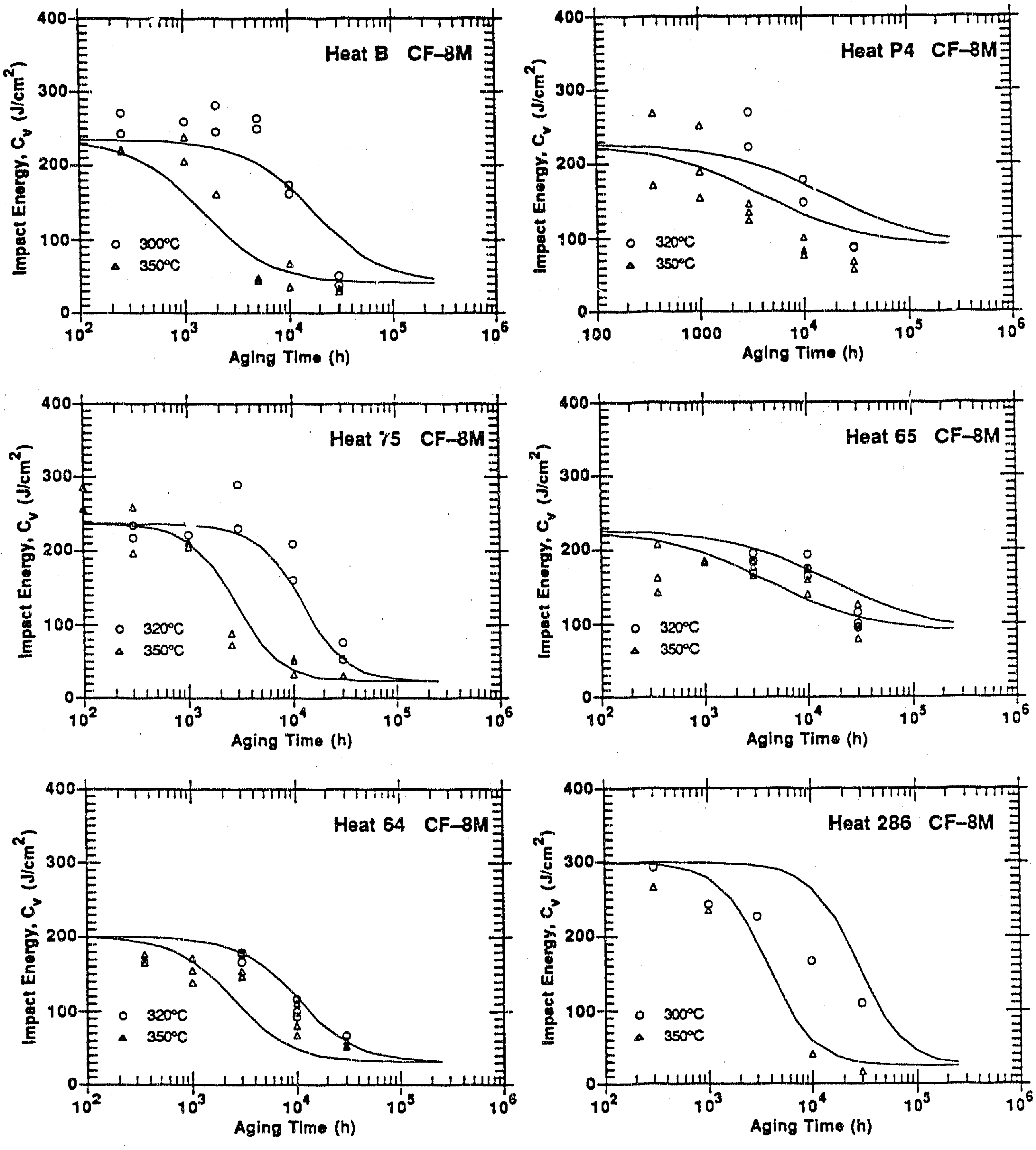

Figure 8. Observed and Estimated Room-Temperature Charpy Impact Energy for Aged CF-8M Cast Stainless Steels.

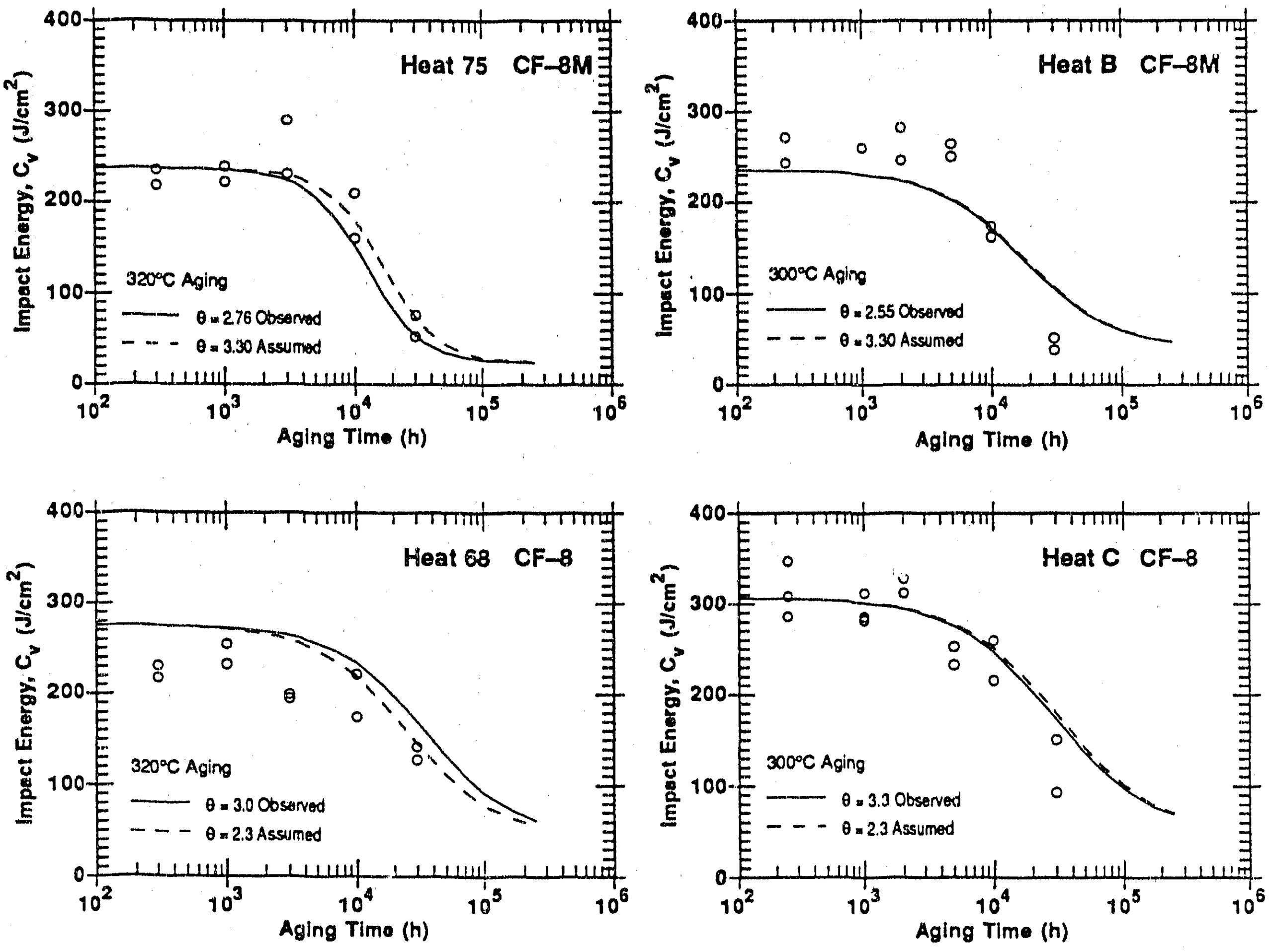

Figure 9. Room-Temperature Charpy Impact Energy for Aged CF-8 and CF-8M Cast Stainless Steels Estimated with Different Values of the Constant θ.

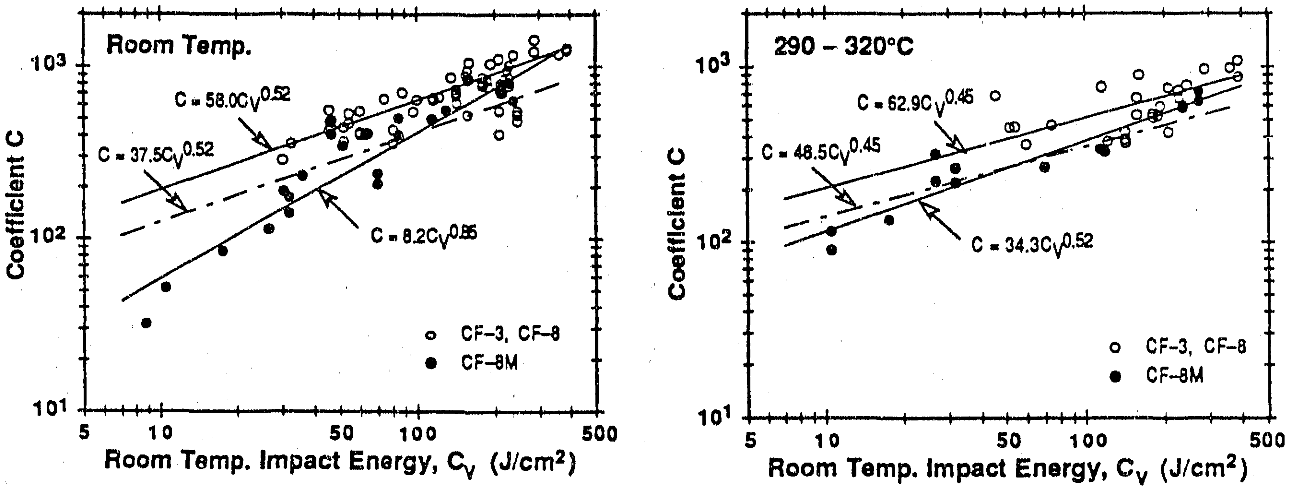

Figure 10. Correlation between Room Temperature normalized Charpy-impact Energy and Coeffiecient C for Cast Stainless Steel at Room Temperature and 290–320°C.

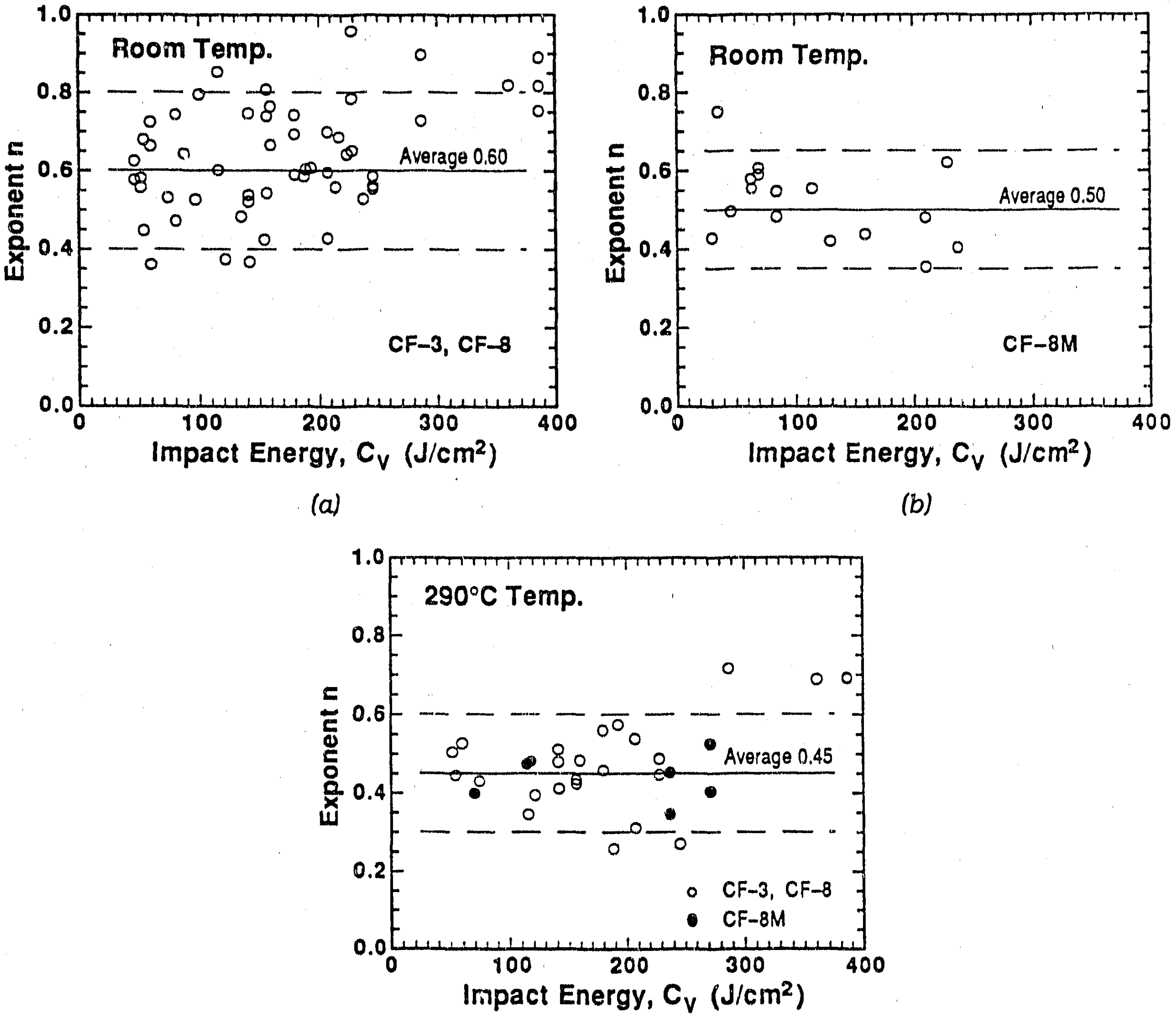

(a)

(b)

(c)

Figure 11. Experimentally Observed Exponents n for Power-Law J-R Curve at (a) and (b) Room Temperature and (c) 290°C for Aged Cast Stainless Steels.

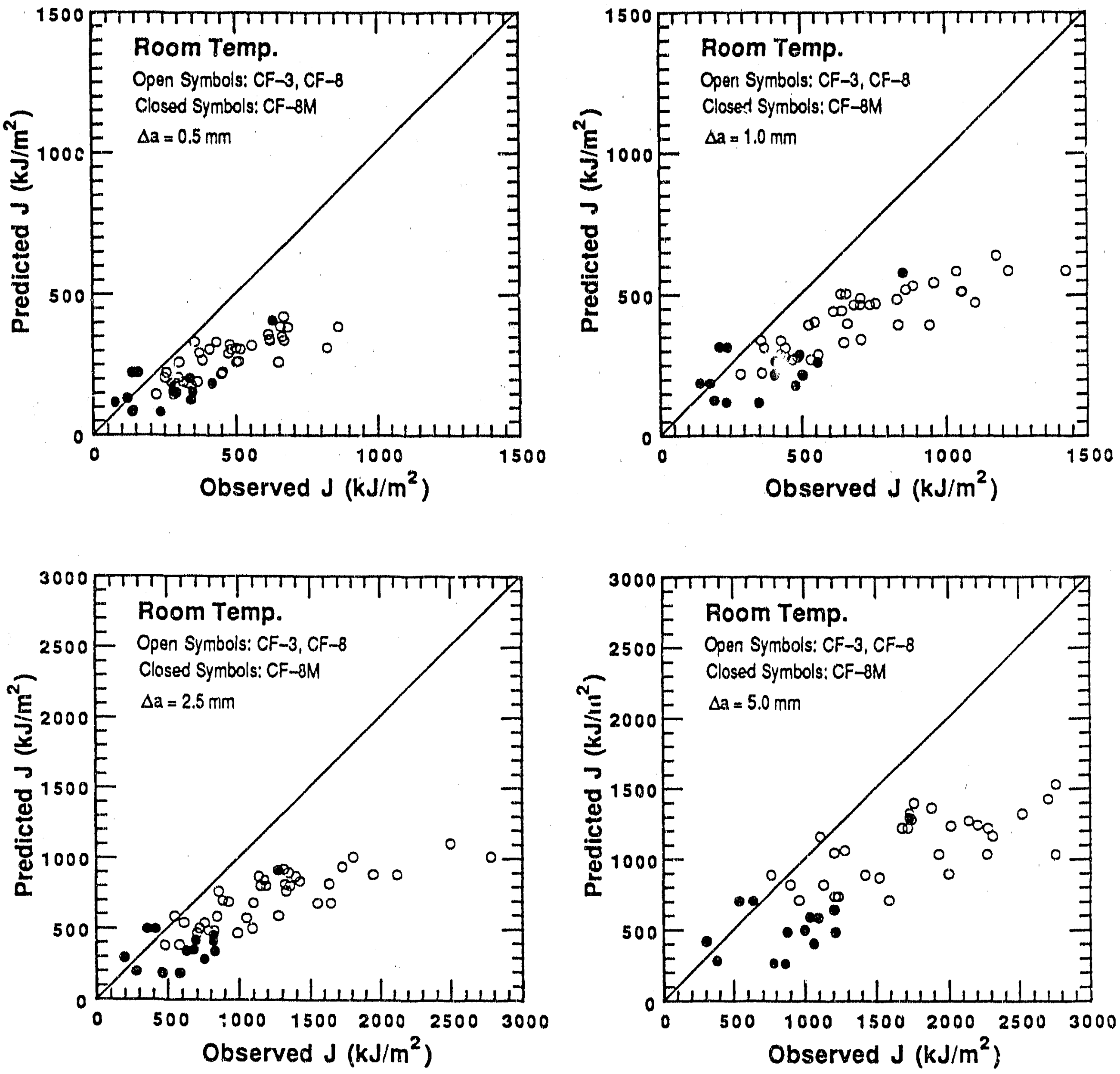

Figure 12. Estimated and Observed J Vaues at Room Temperature and 0.5-, 1.0-, 2.5-, and 5.0-mm-Crack Extension for Aged Cast Strainless Steels. J values estimated from material information (Method A) and the kinetics of embrittlement.

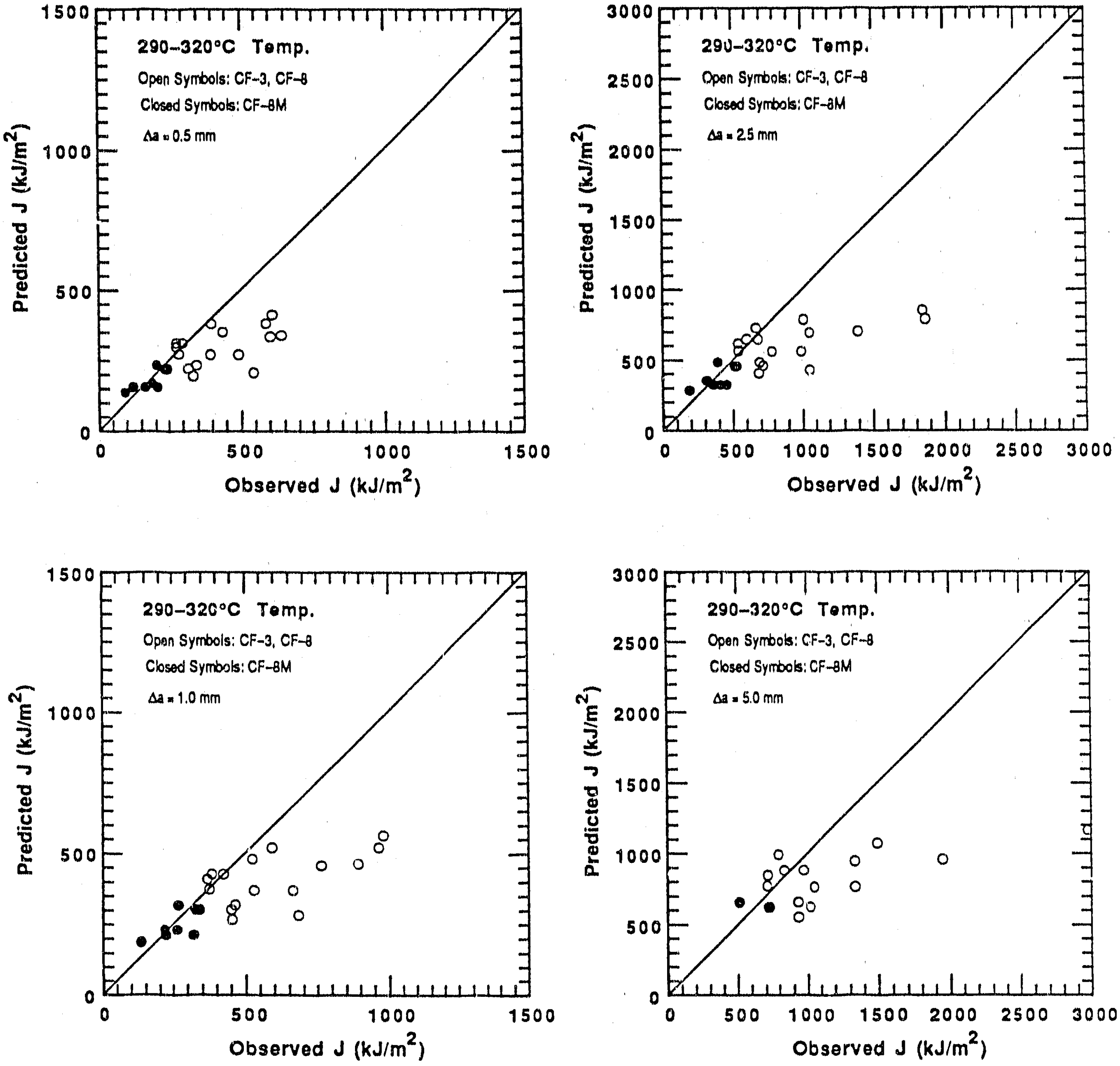

Figure 13. Estimated and Observed J Vaues at 290°C and 0.5–, 1.0–, 2.5–, and 5.0–mm–Crack Extension for Aged Cast Strainless Steels. J values estimated from material information (Method A) and the kinetics of embrittlement.

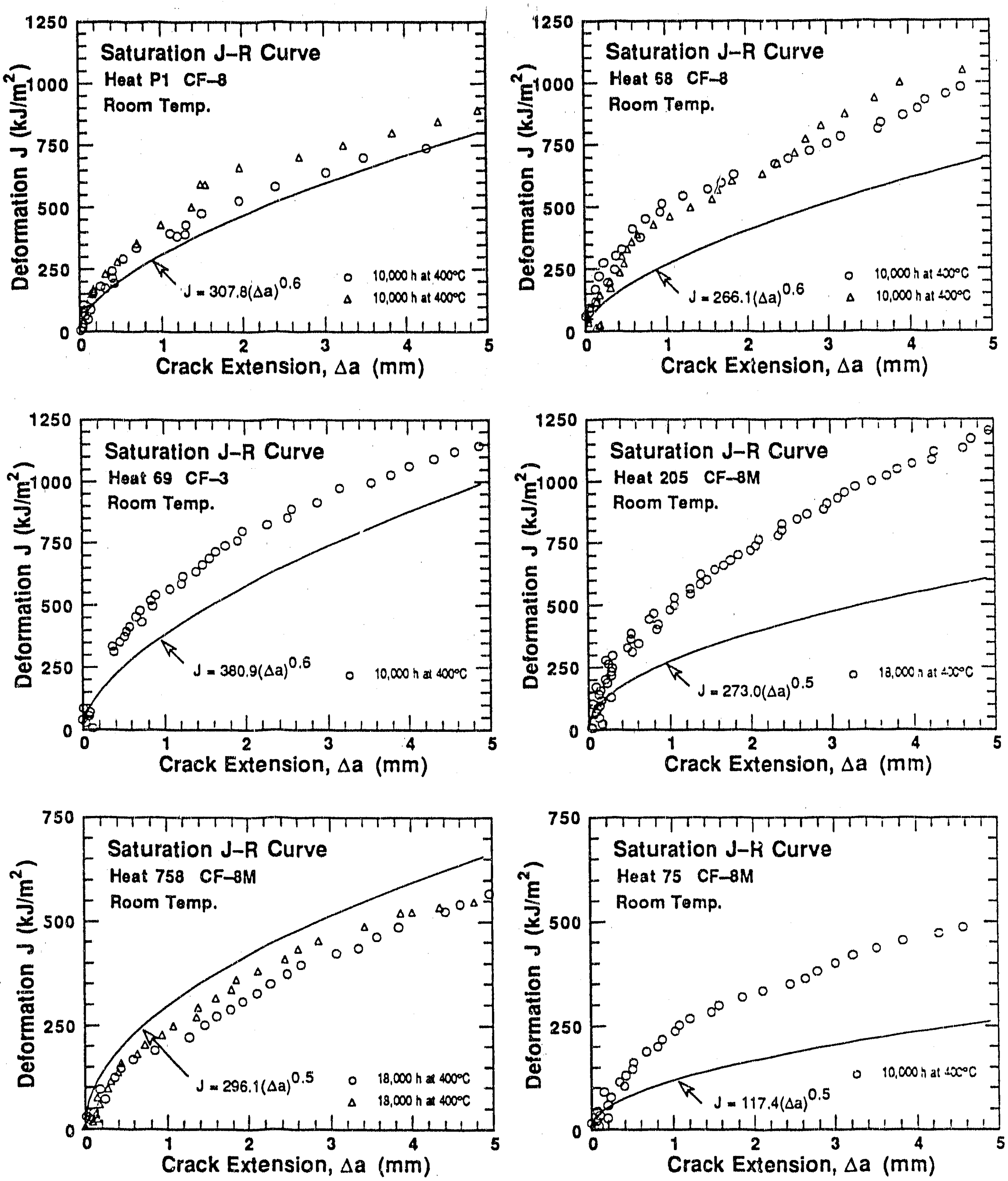

Figure 14. Saturation Fracture Toughness J-R Curve at Room Temperature Estimated by Method A for CF-3, CF-8, and CF-8M Cast Stainless Steels..

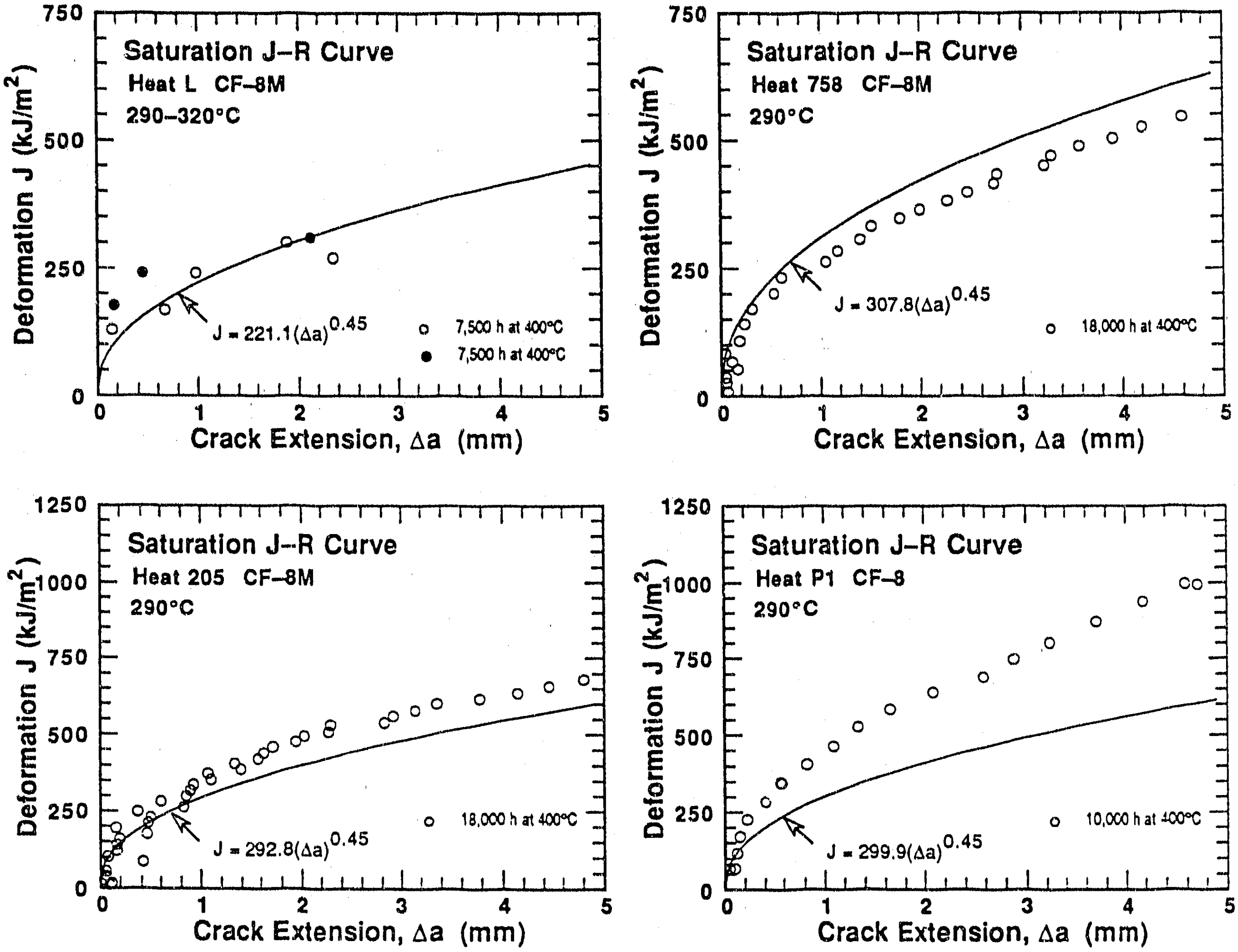

Figure 15. Saturation Fracture Toughness J–R Curve at 290°C Estimated by Method A for CF-3, CF-8, and CF-8M Cast Stainless Steels.

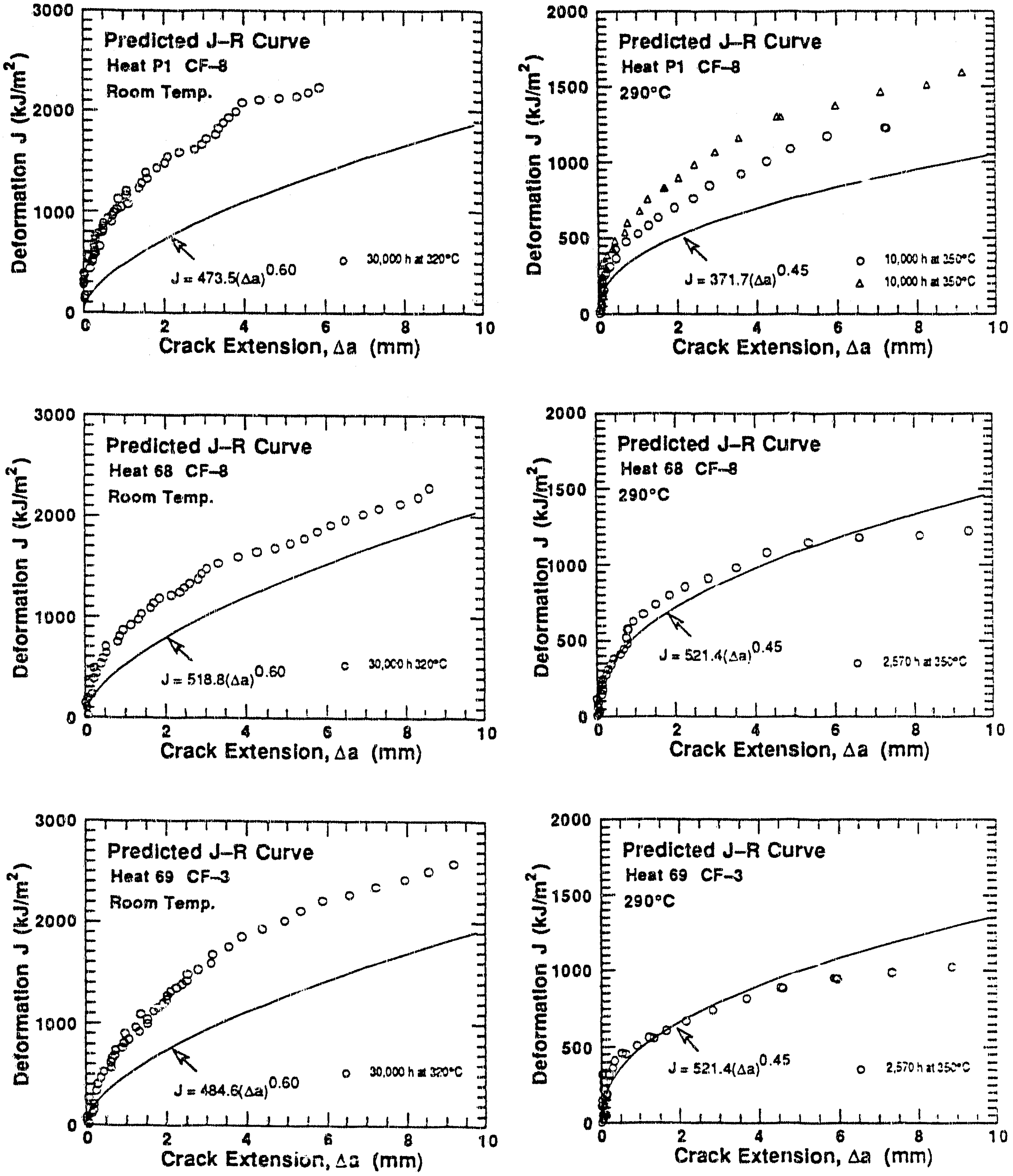

Figure 16. Fracture Toughness J–R Curve at Room Temperature and 290°C Estimated by Method A for Partially Aged CF–3 and CF–8 Cast Stainless Steels.

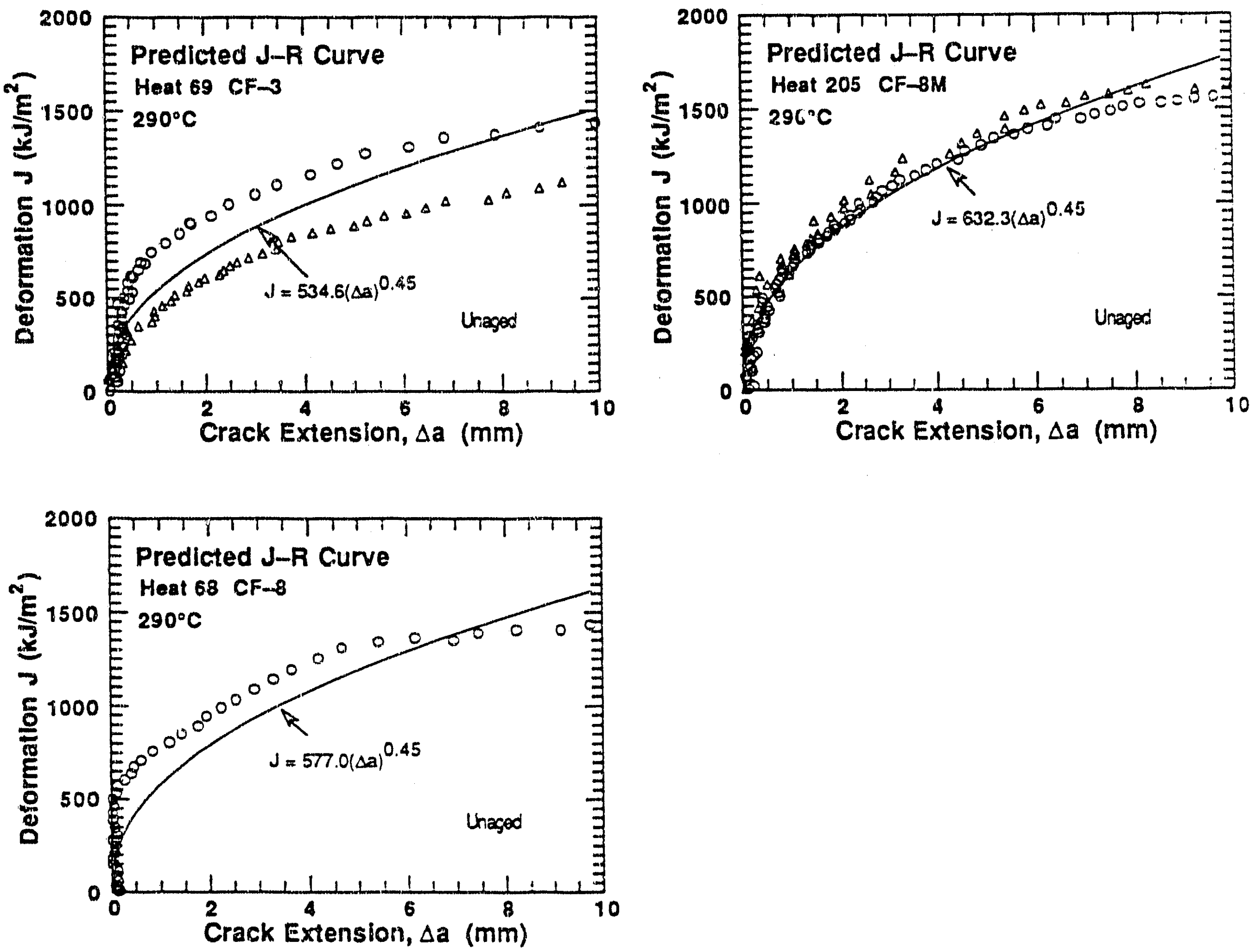

Figure 17. Fracture Toughness J–R Curve at 290°C Estimated by Method A for Unaged CF–3, CF–8, and CF–8M Cast Stainless Steels.

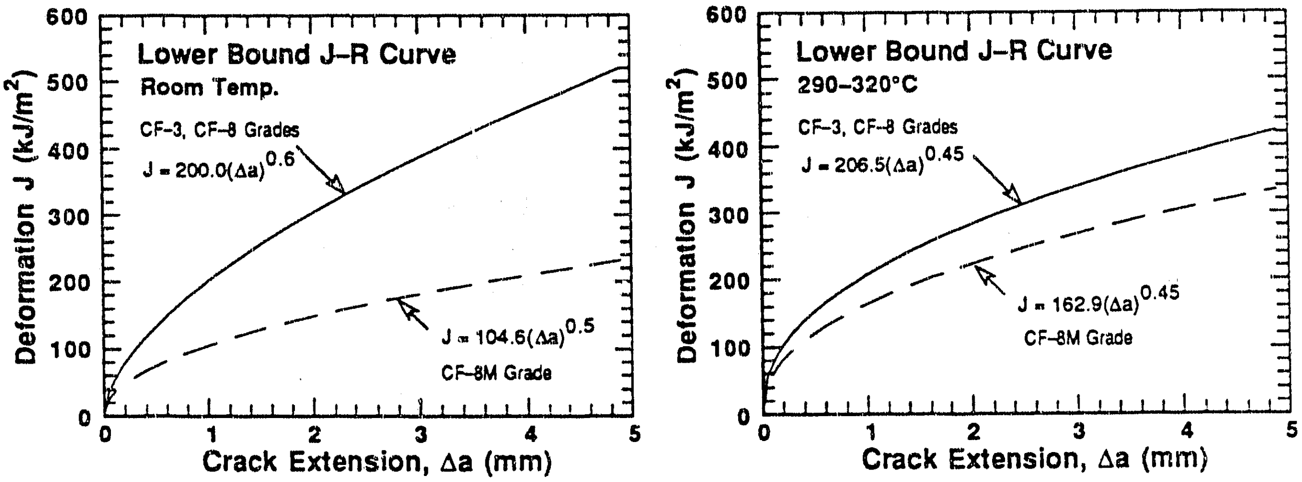

Figure 18. Lower Bound Fracture Toughness J-R Curves at Room Temperatrure and 290–320°C.

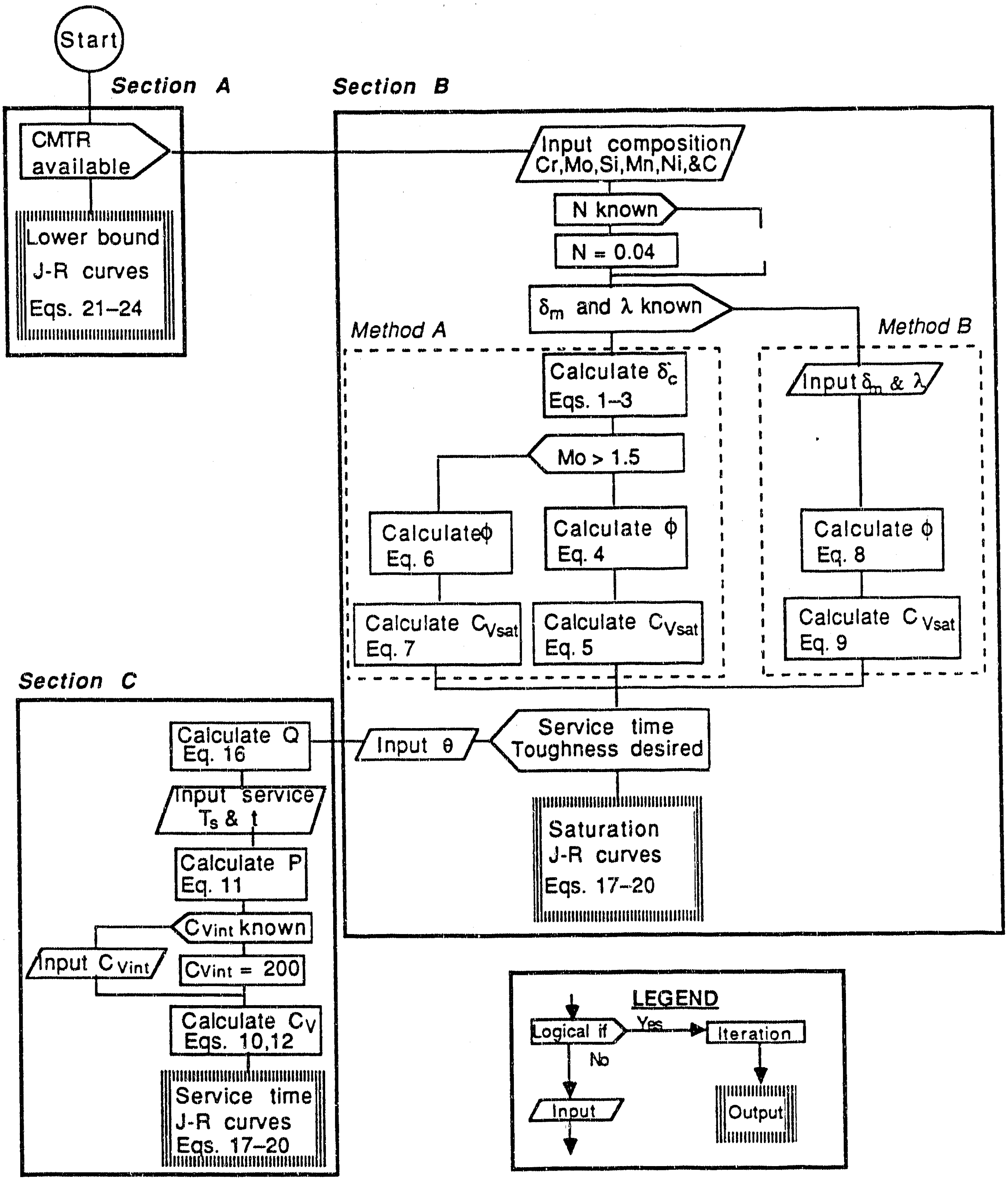

Figure 19. Flow Diagram for Estimation of Fracture Toughness J–R Curves of Cast Stainless Steels in LWR Systems.

END

DATE FILMED

02 / 11 / 91